Kinetics of HCl Uptake on Ice at 190 and 203 K: Implications for the Microphysics of the Uptake Process

Thomas Huthwelker,*,†,‡,§ Maria E. Malmström,†,|| Frank Helleis,† Geert K. Moortgat,† and Thomas Peter‡

Max-Planck-Institut für Chemie (Otto-Hahn-Institut), Joh.-Joachim-Becher-Weg 27, D-55128 Mainz, Germany, and Institut für Atmosphäre und Klima (IACETH), Schafmattstr. 30 ETH-Hönggerberg, CH-8093 Zürich, Switzerland

Received: August 12, 2003; In Final Form: March 10, 2004

The uptake of HCl on vapor-deposited ice is investigated for HCl partial pressure p from 2×10^{-8} to 10^{-5} Torr at temperatures of 190 and 203 K in an especially designed Knudsen cell experiment. Two kinetic regimes can be distinguished experimentally: a long-lasting tailing which accounts for the major amount of the overall uptake and follows diffusion-like kinetics, $\gamma(t) \propto t^{-1/2}$ (γ, uptake coefficient; t, time), and an initial period, where the uptake is higher than predicted by diffusion-like kinetics. The uptake kinetics are analyzed using analytical equations and also by full numerical simulation of simultaneous adsorption onto the surface and diffusion into the bulk. We derive the quantity $H_d^* D^{1/2}$ (H_d^*, effective Henry's law constant, D diffusion constant) and find $H_d^* D^{1/2} \propto p^{-1/2}$, which implies that HCl dissociates upon uptake. The results for both analysis methods closely coincide. We suggest the use of a semiempirical parametrization for the total HCl uptake (molecules per geometric surface area) on vapor-deposited ice films as time dependent function $n(t, p) = n_{resid}(p) + C(T)(tp)^{1/2}$, where $C(T)$ is a constant which depends on temperature only. The compatibility of the residual, nondiffusive uptake, n_{resid}, with various adsorption isotherms is discussed. The analysis suggests that the experimentally observed diffusion-like kinetics dominates the overall trace gas uptake after a brief initial period. The diffusion-like kinetics must be considered when analyzing uptake experiments and when making applications to natural ice.

Introduction

The uptake of trace gases on ice is of great importance for several environmental problems. Heterogeneous reactions of halogen species on ice particles play a key role in the formation of the springtime ozone hole.[1] Also, the chemical composition of polar ice cores is used to reconstruct Earth's past climate.[2,3] The assessment of both requires a good understanding of the incorporation mechanism of trace gases in and on ice, concerning either the uptake of trace gases on atmospheric ice crystals and snowflakes or processes in polar surface ice.[4]

A specific example for the importance of the HCl interaction with aerosols are heterogeneous reactions of halogen compounds on polar stratospheric clouds (PSC) during polar winter. Reactions such as

$$ClONO_2 + HCl \rightarrow Cl_2 + HNO_3 \qquad (1)$$

on ice surfaces prime the atmosphere for the springtime ozone hole. The reaction mechanism on liquid aerosols is well understood in terms of solubility, diffusivity, and chemical reactions in the liquid phase.[5−8] Conversely, an adsorption mechanism is assumed when implementing the interaction of trace gases on solid aerosol surfaces in atmospheric models.[9−11] However, there are considerable inconsistencies between the available experimental data sets.[12] Therefore, the investigation of the nonreactive uptake of trace gases on ice (i.e., without reaction with another trace gas on the ice surface) is a prerequisite to gain insight into basic physical processes of heterogeneous chemical reactions.

The nonreactive interaction of HCl with ice has been subject of many studies.[13] Early studies focused on the solubility of HCl in ice[14] and the partitioning of HCl between ice and an aqueous HCl solution.[15−17] Later, the solubility and diffusivity of HCl and HNO_3 in single crystals was studied.[18−20] The uptake of gaseous HCl onto vapor-deposited and polycrystalline ice was studied in Knudsen cell experiments[21−24] and flow tube experiments[25−30] and by using other techniques.[31] These studies typically yielded a 0.1−1 monolayer coverage of HCl at the ice surface (see below, i.e. Table 4).

However, despite similar total amounts of the uptake, the dependence on partial pressure and the influence of the ice film thickness on the HCl uptake is yet unresolved. For example, Chu et al.[27] found the total uptake to be proportional to the square root of the HCl partial pressure, while Hanson and Ravishankara[26] reported no dependence on partial pressure ranging from about 4×10^{-8} to 10^{-6} Torr, and Hynes et al.[30] observed a slight increase of the uptake when the HCl partial pressure rose from 3×10^{-7} to 2×10^{-6} Torr.

* Corresponding author. E-mail: Thomas.Huthwelker@psi.ch.
† Max-Planck-Institut für Chemie, (Otto-Hahn-Institut), Joh.-Joachim-Becher-Weg 27, D-55128 Mainz, Germany.
‡ Institut für Atmosphäre und Klima (IACETH), Schafmattstr. 30 ETH-Hönggerberg, CH-8093 Zürich, Switzerland.
§ Current address: Paul Scherrer Institute, CH-5232 Villingen PSI, Switzerland.
|| Current address: Industrial Ecology, Chemical Engineering and Technology, Royal Institute of Technology (KTH), SE-10044 Stockholm, Sweden.

10.1021/jp0309623 CCC: $27.50
Published on Web 07/02/2004

The total HCl uptake was found to rise[27,28] with the film thickness of vapor-deposited ice, which has been interpreted as being caused by the porosity of the vapor-deposited ice film.[27,28,32,33] However, the possible influence of the ice porosity on the trace gas uptake and the chemical reactivity remains controversial.[34,35] Flückiger et al.[22] investigated the diffusion of HCl into ice by titrating with gaseous $ClONO_2$ and invoked a HCl surface layer to explain the experimental results. Moreover, they argued that the HCl uptake may depend on the degree of polycrystallinity of the ice studied. The possible influence of the ice morphology on the HCl uptake has also been demonstrated[36] at temperatures around 173 K.

The trace gas uptake onto ice has been studied using flow tubes by measuring the temporal development of the trace gas concentration at the flow tube exit as a function of time, the so-called breakthrough curve. For HCl[27,30,37] and HNO_3[38] uptake on ice in flow tube experiments and also for SO_2 uptake into packed ice beds[39,40] at temperatures above 243 K, a long-lasting tailing of the breakthrough curves has been observed. In contrast, other flow tube experiments on SO_2 uptake at 190 and 228 K did not reveal long tailing,[41,42] though the small magnitude of SO_2 may have prevented this. This tailing reflects a slow, long-lasting interaction process between the trace gas and the ice surface. The nature of this process is yet unknown, but it has been recognized that the tailing would be consistent with diffusive kinetics for HNO_3 uptake on vapor-deposited ice[38] and SO_2 in packed ice bed experiments.[43,44]

The overall trace gas uptake is often conveniently specified as "uptake per surface area". To derive the total uptake from the breakthrough curve, it is crucial to determine the end of the uptake process, which can be difficult in the presence of the tailing. One method used to define the uptake in flow tube experiments is to integrate the total uptake until the breakthrough curve rises to two-thirds of its original value.[30,38] However, as long as the nature of the tailing is not yet understood, there is no physically well-defined criterion to define how to handle the tailing when interpreting the breakthrough curve in uptake experiments. The fraction of the uptake related to the final third of the relaxation of the breakthrough curve can in principle be arbitrarily larger than the fraction of the uptake during the leading two-thirds.

Additional complications arise from the specific nature of the ice surface, its extremely dynamic character (at 200 K about 1000 monolayers of ice are exchanged with the gas-phase per second), and the presence of a disordered surface layer, or quasi-liquid layer (QLL). The QLL is well-known to exist on metals[45] and on ice[46−53] at temperatures close to the melting point. However, recent spectroscopic studies suggest that surface disorder may already exist at temperatures as low as 200 K[54] on pure ice. While it has been hypothesized that trace gases might be taken up into the QLL,[25,55−59] there is still considerable debate around this topic.[58,60−63]

A confined reservoir, similar to the QLL, is the grain boundaries in polycrystalline ice. The line where three grains meet is a so-called triple junction or vein. The negative curvature of the physical surface in a triple junction thermodynamically stabilizes supercooled water,[64] comparably to surface forces, which stabilize the QLL.[53] The existence of liquid aqueous solutions has been shown experimentally[65,66] in triple junctions of polycrystalline ice and in the necks of adjacent ice spheres.[67] Triple junctions may serve as reservoirs for impurities. For example, sulfuric acid has been found in the triple junctions of polar ice[68] and HCl has been localized in triple junctions of laboratory ice which was exposed to gaseous HCl.[69]

Infrared spectroscopy has been used to show the existence of the ions on the ice surface in the presence of acidic vapors,[23,70−73] mostly at partial pressures sufficiently high to melt the ice or to form hydrates. Devlin et al.[74] found that the HCl first attached to the dangling bonds and then dissociates by donating the proton to a water molecule on the surface to form an H_3O^+ ion. This work is consistent with a recent ab initio study of the HCl ice interaction[75] which showed that the HCl molecule first develops three bonds binding to the ice surface and that the subsequent ionization of HCl on the ice surface has no energetic barrier. Molecular dynamics simulations, which take the dynamic nature of the ice surface into account, suggest that the HCl molecule may be built into the hexagonal ice, where it acts as a proton donor and dissociates.[76] It is important to note that these theoretical models do not invoke a QLL as necessary to explain the dissociation of HCl on ice.

The variety of conceivable processes and reservoirs hampers a clear understanding of the uptake process and renders interpretation of uptake experiments difficult. Bulk and/or surface processes may govern the HCl uptake on ice simultaneously. In this paper, we study the kinetics of the HCl uptake on ice as a function of the HCl partial pressure using a newly developed Knudsen cell experiment and test various hypotheses to interpret the experimental observations.

Basic Concepts for Trace Gas Uptake

To provide concepts for the interpretation of HCl uptake experiments, we recall basic physical concepts to describe the uptake of trace gases on ice. In the first uptake step, HCl molecules may be adsorbed onto the ice surface. This process can be modeled using adsorption isotherms, which express the amount of trace gas taken up onto a surface (n_{surf} in molecules/cm^2) as a function of the gas-phase partial pressure p. The simplest isotherm is the Freundlich isotherm, which assumes a relationship of the form

$$n_{surf} = \text{const} \times p^j \tag{2}$$

where j is an empirical constant. More sophisticated adsorption models, such as the Langmuir or the BET isotherms (for a review, see Adamson[77]) have also been used to describe uptake processes on ice.[9,10,12,78−80]

Bulk processes can be described by diffusion and bulk solubility. The latter can be expressed by the dimensionless Henry's law constant, H_d, which assumes the linear relationship

$$H_d \frac{p}{k_B T} = n \tag{3}$$

between the vapor pressure of the gas, p, and molecular density in the ice phase, n, of the dissolved gas in the condensed phase at temperature T; k_B is the Boltzmann constant.

Upon uptake onto ice, a fraction of the HCl molecules dissociates.[74] Thus, the overall solubility is governed by two coupled equilibria: the molecular solubility and the dissociation equilibrium, which can be described by the effective Henry's law constant

$$H_d^* = \frac{n_{HCl,tot}}{p_{HCl}} k_B T \tag{4}$$

Here is $n_{HCl,tot} = n_{HCl} + n_{Cl^-}$, where n_{HCl} and n_{Cl^-} represent the undissociated and dissociated HCl densities in the condensed phase, respectively. For pure ice, that is in absence of other proton donors, electroneutrality and the law of mass action for

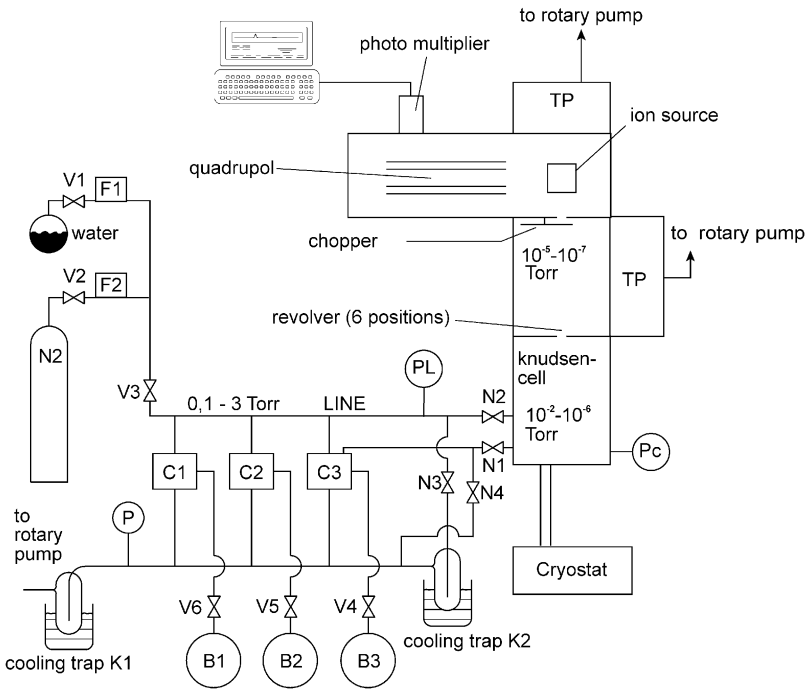

Figure 1. Experimental setup. Key: F1 and F2: mass flow controller (MKS); V1−V6: valves; C1−C3: flow controller; P_L and p_c: pressure measurement in line and Knudsen cell, respectively; TP: turbopump; B1−B3: supply for the trace gas mixtures.

dissociation read $n_{H^+} \cong n_{Cl^-}$ and $n_{Cl^-}{}^2/n_{HCl} \cong K$, respectively. Thus, the effective Henry's law constant takes the form

$$H_d^* = H_d + \sqrt{\frac{KH_d k_B T}{p_{HCl}}} \approx \sqrt{\frac{KH_d k_B T}{p_{HCl}}} \tag{5}$$

in which H_d is the intrinsic Henry's law constant (according to eq 3) and K is the dissociation equilibrium constant. This leads to the proportionality $H_d^* \propto p^{-1/2}$ in the case of a completely dissociating species.

To describe uptake kinetics in a Knudsen cell, we note the flux density j of an ideal gas at a partial pressure p onto a surface

$$j = \frac{p}{\sqrt{2\pi m k_B T}} \tag{6}$$

Here m is the molecular mass of the molecule.

A molecule hitting the surface will be accommodated on the surface with probability α_c (mass accommodation coefficient). The mass accommodation limits the uptake kinetics only in the initial stage of the uptake process.[81] Due to surface saturation, diffusive uptake limitations, and desorption into the gas phase, the net fraction of molecules taken up onto the surface is lower than α_c. This experimentally measurable net-uptake is described by the uptake coefficient

$$\gamma \equiv \frac{\text{no. of molecules taken up on the surface}}{\text{no. of molecules hitting the surface}} \tag{7}$$

which can be time-dependent. Fundamental physical constants must be derived from the measured uptake coefficient by applying appropriate theoretical models to analyze the measured value for γ.

The uptake coefficient of a diffusing species in the Knudsen cell is

$$\frac{1}{\gamma(t)} \simeq \frac{\bar{v}}{4}\frac{\sqrt{\pi t}}{H\sqrt{D}} + \frac{1}{\alpha_c} \tag{8}$$

See Appendix A. If the species completely dissociates upon dissolution, the relation

$$\frac{1}{\gamma(t)} \simeq \frac{\bar{v}}{4kT_S}\sqrt{\frac{p_r(t)}{KH_{d,0}}}\sqrt{\frac{\pi t}{D}} + \frac{1}{\alpha_c} \tag{9}$$

replaces eq 8 (see Appendix A), where T_S is the substrate temperature, $\bar{v}$ the mean thermal velocity, and $p_r(t)$ the trace gas partial pressure in the Knudsen cell during uptake. In eq 9, the time dependence of p_r accounts for the change of the effective Henry's law constant (see eq 4) during initial reduction and subsequent recovery of the partial pressure after the plunger has been opened. In the following we use expression 9 without the mass accommodation term ($1/\alpha_c$), which can be safely neglected for all but the first instances during uptake.

Experimental Section

The experimental setup (Figure 1) as used in this study consists of three parts: the gas mixing unit, the Knudsen cell, and the quadrupole mass spectrometer.

The gas mixing unit (lower left part in Figure 1) serves to establish fluxes of water and HCl vapor through the Knudsen cell. Partial pressures range from 10^{-4} to 10^{-3} Torr of H_2O and from 10^{-8} to 10^{-5} Torr of HCl. The Knudsen cell and the gas mixing unit are manufactured completely out of glass to minimize memory effects of the trace gases on the walls.

Construction of the Knudsen Cell. Figure 2 sketches the Knudsen cell, which consists of two glass pieces. The upper part is connected to the mass spectrometer and the gas mixing unit. The lower part hosts the cooled sample holder. There are two inlets for the trace gases (water and HCl). The mount for the pressure head (MKS Baratron, 0.1 Torr) is located directly above the ice substrate, perpendicular to the gas flux through the cell. The substrate can be covered by a plunger, which hangs on a glass rod. This rod is fed through a remodeled Young valve, which is fused into the roof of the cell. Using the thread of the Young valve, the plunger can be pressed down to seal the

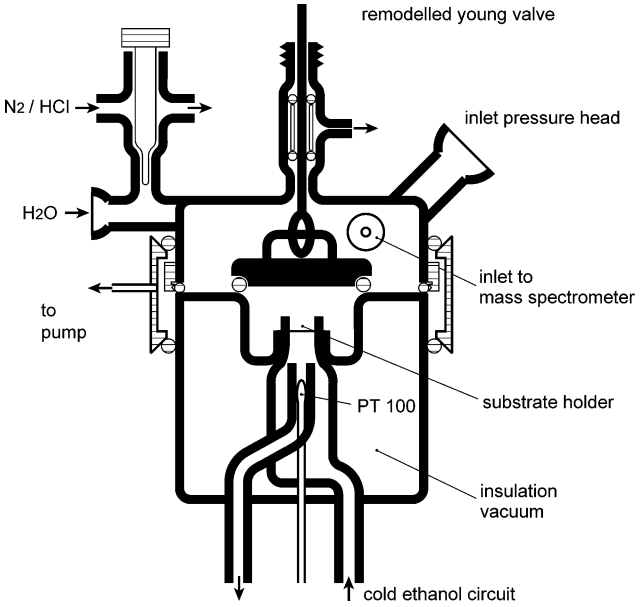

Figure 2. Schematic diagram of the all-glass Knudsen cell. The upper part shows the inlets for the trace gas and water vapor, as well as the plunger which is mounted in a Young valve, which is fused into the top. The lower part hosts the thermostated substrate holder.

substrate surface from the cell with an Viton O-ring. The substrate holder is located in the lower part of the Knudsen cell. It is cooled by a liquid ethanol circuit, which is cryostated using a commercial cryostat (Huber 420). The temperature is measured using a platinum temperature sensor in the ethanol circuit just below the substrate holder.

Preparation of the Water Flux. Deionized water, which was degassed by several freezing/melting cycles, is used as the water vapor source. The water vapor is pumped from the water reservoir via valve N3 into the liquid nitrogen cooling trap K2 (cf. Figure 1). The water vapor flux is regulated by a commercial gas flow controller (MKS). This technique maintains a constant water pressure P_L in the line and the Knudsen cell. A small portion of the water vapor enters the Knudsen cell via valve N2. All valves are thermostated to about 40 °C to ensure stability against temperature changes in the laboratory. The stability of the water vapor flux is better than 0.5% over 10 h, allowing precise long-duration experiments.

HCl Flux. Gaseous HCl is taken from a lecture bottle and diluted with nitrogen (typical mixing ratios ranging from 1:20 to 1:2000). The gas mixture is stored in a glass bulb (B3) and flowed via a gas flow controller (C3) and valve N4 into the cooling trap K1. A small part of this flux is bled through the needle valve N1 into the Knudsen cell. This technique allows a fast conditioning of the flow system, while fluxes into the Knudsen cell are small.

Mass Spectrometer. Partial pressures in the Knudsen cell are measured using a quadrupole mass spectrometer (Balzers, Type QMA 410). The cell is connected to the mass spectrometer via a differential pumping stage. Pinholes of six different hole sizes with diameter ranging from 0.7 to 10 mm allow the gas flux into the spectrometer to vary. Measured escape rates for nitrogen are 15.3 (hole 6), 3.9 (hole 5), and 1.01 s^{-1} (hole 4).

Molecules are ionized by electron impact and analyzed in the quadrupole. In the differential pumping stage, there is a chopper wheel, which interrupts the gas flow with a frequency of 700 Hz. Signal analysis with a digital lock-in amplifier allows a direct subtraction of the signal background during measurement.[82] This technique was necessary to eliminate wall effects in the mass spectrometer.

Because the amount of HCl in the water vapor is small, water was monitored on the weak $m/e = 20$ (H_2O^{18}) fragment, and HCl on its main line $m/e = 36$. The mass spectrometer was calibrated in the following manner. For each gas, the mass spectrometer signal was measured as a function of the partial pressure in the cell (i.e., $p_i = S_i I_i$, with p_i = partial pressure, I_i = mass spectrometer signal, S_i = sensitivity, all for species i). Water vapor was calibrated with pure water vapor in the cell; for HCl, different HCl/N_2 mixtures of known composition were used. The absolute sensitivity S_i of the mass spectrometer was measured on the same day, to avoid possible influences of the daily change in sensitivity. This procedure was repeated on different days and the relative sensitivity $S_r \equiv S_{20}/S_{36}$, was determined. For the following analysis we use the average value of $S_r = 0.0225 \pm 15\%$. This error represents an upper limit estimated from the reproducibility of the S_r under different pressure conditions in the mass spectrometer.

On each day, when an uptake experiment was performed, the absolute sensitivity for water on the $m/e = 20$ fragment was determined. Then the ice vapor pressure was measured in each experiment. The temperature of the ice has a higher absolute reproducibility and stability in the experiment compared to the absolute setting of the water vapor pressure. Therefore, the ice vapor pressure is the ideal absolute reference point for the MS calibration. For each temperature, we determined the average value $\bar{p}_{vap,ice}(T)$ of all measured ice vapor pressures, which was adopted as best estimate of the ice vapor pressure at the given temperature. Once the absolute sensitivity was determined, we calculate the HCl partial pressure from the $m/e = 36$-line using the relative sensitivity S_r. By this calibration procedure, we make all measured HCl pressures consistent, i.e., independent of the day by day changes of the mass spectrometric sensitivity.

Ice Growth and Ice Vapor Pressure Measurement. Ice was grown on the glass substrate holder. First, with closed plunger, a flux of water vapor was passed through the Knudsen cell. The ice film was nucleated with several short events of opening and closing the plunger to avoid any formation of ice islands on the glass substrate holder. Then the plunger was left open for about 1 h to grow the film at a temperature of 190 K. Vapor-deposited ice under these conditions is known to consist of many individual micrometer sized grains of hexagonal ice.[28,32] The internal surface area may be about 10 times higher as the geometric surface area.[28,78]

Water and HCl background partial pressures were monitored during the ice growth to estimate the ice film thickness and the maximum contamination of the ice by background HCl in the cell (typically $10^{-8}-10^{-9}$ Torr), resulting from previous experiments. Because of the fast ice growth, the HCl uptake was kinetically limited, thus, the HCl contamination in the ice was well below the equilibrium solubility of HCl in ice at background pressures. Partial pressures used in the experiments were chosen about 2 orders of magnitude above the HCl-background pressures; therefore, the HCl background concentration does not influence our results. The only exception were experiments at very low HCl partial pressures of about 10^{-8} Torr. Here, the initial HCl background pressure during the ice growth was about 10^{-9}, close to the mass spectrometric detection limit. Film thicknesses are typically between 5 and 30 μm as calculated from the total amount of deposited water and the geometric surface area. The maximum HCl mixing ratio x in the ice has always been well below $x^i_{HCl} < 10^{-7}$, for details see ref 83.

Procedure of Uptake Experiments. After the growth of the ice film was complete, the ice was brought to the desired

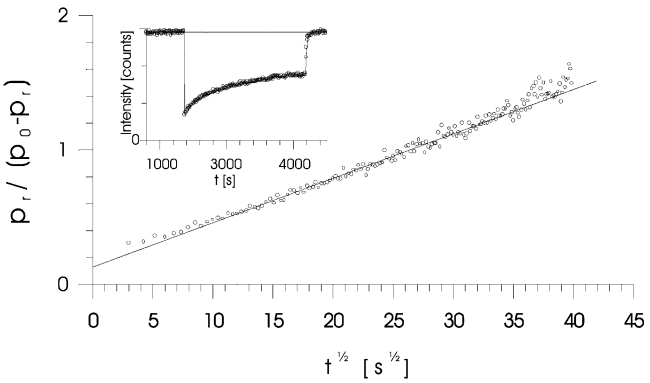

Figure 3. HCl uptake on 60 wt % H_2SO_4-solution at 203 K evaluated according to eq 20; *x* axis: experimental time; *y* axis: $p_r(t)/(p_0 - p_r(t)$. Inset: Raw data. The plunger was opened at 1350 s ($t = 0$) and closed again at 3200 s.

experimental temperature with closed plunger. Then, the water flux through the cell was manually adjusted until no change in water partial pressure occurred upon opening and closing the plunger. By this method, the ice vapor pressure can be measured. As described in Appendix A, the measured water vapor pressure was corrected to account for different temperatures of the ice substrate and the pressure head (cf. Equation 28). Because the walls of the Knudsen cell are at room temperature, the sample surface temperature is slightly higher than the temperature at the temperature measured by a PT 100-sensor in the cell just below the substrate. At ~190 K, comparison of the vapor pressures measurements with the parametrization of McDonald[84] shows that the ice substrate is no more than 1−2 K warmer than that measured at the temperature sensor. For better accuracy, the ice temperature was always derived from the measured water vapor pressure.

After ice preparation, the HCl uptake was studied. With the plunger still held closed, an HCl flux was introduced into the cell. Care was taken to allow stabilization of the HCl flux through the cell. Since we aimed to study the HCl uptake over long time periods, we considered a change of at most a few % in the HCl partial pressure during the course of an uptake experiment as acceptable. After the stabilization period the pressure p_0 was established in the cell, the plunger was opened, and the HCl partial pressure p_r was monitored as a function of time for periods between 10 min and several hours. Then, the plunger was closed, and p_0 was remeasured to test for possible drift of the HCl partial pressure.

Error Analysis. The error in the HCl partial pressure was determined from the standard deviation of the averaged partial pressure data before and after opening the plunger. If the HCl drift was bigger than the calculated standard deviation, we use the drift as error for the pressure. This error estimate does not take systematic errors of the calibration into account. The measurement of the HCl partial pressures is based on the relative sensitivity of the lines for water ($m/e = 20$) and HCl ($m/e = 36$). This value has been determined experimentally, with an absolute error of about ±15%.[85]

HCl Uptake on Sulfuric Acid Solutions. To test the newly developed experimental system, we performed HCl uptake experiments on 60 wt % sulfuric acid solutions at 203 K. Under these conditions, diffusion into the liquid phase is the well established dominant process.[6,7] Figure 3 shows an example of $1/\gamma$ vs $1/\sqrt{t}$. Analysis of the data, using eq 20, yielded 8.1 ± 2.7 M atm^{-1} $s^{-1/2}$, which, within errors, agrees well with the value reported by Williams and Golden.[86] No dependence of the determined $H_d\sqrt{D}$ values on p_{HCl} or on pinhole setting was detected (data not shown). These results are one example verifying the performance of the experimental system.

Results

A typical uptake experiment is illustrated in Figure 4a, where we show the raw data of mass $m/e = 36$, as measured with the mass spectrometer. Initially, the plunger is closed. After opening the plunger at $t = 0$, the HCl signal drops and recovers slowly with time. After 3000 s, the plunger is closed and the HCl partial pressure slowly rises back to its original value.

Long-lasting tailing, such as shown in Figure 4a has been observed previously when investigating the uptake of acidic gases on ice[25,27,30,38] in flow tubes. It has been pointed out by Abbatt[38] that the tailing could possibly be consistent with the kinetics of a diffusion process. The tailing makes it difficult to determine the total HCl uptake. As a practical approach in flow tube experiments, a two-thirds criterion has been invoked to estimate the overall uptake on ice by ignoring any uptake after two-thirds of the original signal is reestablished.[30,38] In the following, we test the compatibility of different physical models with the experimental data, by using analytical and numerical modeling and application of the two-thirds criterion to our Knudsen cell experiments.

In our experiments, the stability of the HCl flux into the cell is typically better than a few percent drift during the course of one experiment. However, to safely exclude the potential influence of any small HCl drift on the data analysis, we determine the drift by fitting a straight line ($p_0(t) = a + bt$) to the measured HCl partial pressure data before opening and after closing the plunger. This line is used to normalize the data by calculating $p_r(t) = [p_{r,exp}(t)/p_0(t)] \times \bar{p}_0$. Here $p_{r,exp}(t)$ is the experimentally measured HCl partial pressure during uptake; $\bar{p}_0$ is the average partial pressure during the experiment. This drift-corrected HCl partial pressure is shown in Figure 4b.

Asymptotic Model. Figure 4c shows $1/\gamma(t)(p_0/p_r(t))^{1/2}$ as a function of $t^{1/2}$ to test the validity of relation 9, which describes the diffusive uptake of a dissociating trace gas. The linearity holds for $t_{as}^{1/2} > 30$ $s^{-1/2}$. The quantity $H_d^* D^{1/2} = (k_B T_S K H_d D/p_0)^{1/2}$ was calculated by fitting eq 22 to the data (for $t > 900$ s) and is used to plot $p_r(t)$ (as calculated from eq 23 in Appendix A) in Figure 4b (dotted line). As relation 22 describes the data asymptotically, we call this evaluation method the "asymptotic model". Note that the mass accommodation coefficient (eq 9) has no influence on the asymptotic fitting. Figure 4b shows that the asymptotic model is consistent with the data for $t > 900$ s. However, there is considerable deviation during $t < 900$ s the HCl uptake is higher than predicted by the asymptotic model.

In Figure 4d, we plot the total HCl uptake n_{tot} as a function of $t^{1/2}$ (Figure 4d, open circles, eq 25, with p_r taken from the raw data). The linearity $n_{tot} \propto t^{1/2}$ emphasizes the diffusive kinetics of the uptake process and, most importantly, experimentally shows that the long-lasting HCl uptake on ice is slow, but without apparent saturation.

Once, $(k_B T_S K H_d/p_0)^{1/2}$ has been determined for the asymptotic model, a first approximation of the diffusion-like component can be calculated by numerical integration of eq 25, with R_S from eq 16 and p_r from eq 23. This is shown as dotted line (labeled as "diffusion like") in Figure 4d. The residual $n_{resid}(t)$, which remains unexplained by the diffusion-like kinetics, can be calculated by $n_{resid}(t) = n_{tot}(t) - n_{diff}(t)$ (Figure 4d, dotted line, (labeled as "nondiffusive"). As expected, the nondiffusive component $n_{resid}(t)$ becomes independent of time for $t > 900$ s.

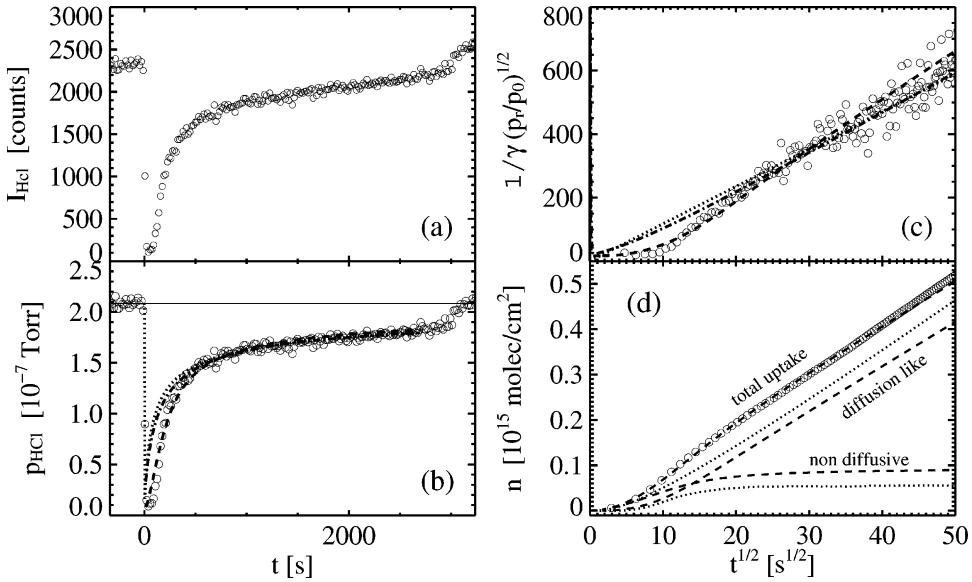

Figure 4. Evaluation of an HCl-uptake experiment at a temperature of 188 K. (a) Raw data of a typical uptake experiment. The signal drops, when the plunger is opened ($t = 0$). At $t = 3000$ s, the plunger is closed and the HCl signal recovers to its original value. (b) Raw data converted to HCl partial pressure units and normalized as discussed in the text. (c) $1/\gamma(p_0/p_r)^{1/2}$ as a function of $t^{1/2}$. (d) Total, diffusion-like, and nondiffusive uptake per surface area as a function of $t^{1/2}$. Key for all parts: circles: experimental data; dotted line: asymptotic model (eq 22); dashed line: full numerical model (Appendix B); dash−dotted line: numerical model without surface uptake $\theta_{equi} \cong 0$.

The time independence of $n_{resid}(t)$ for $t > t_{as}$ allows to estimate the overall contribution of n_{resid} to the uptake by taking the average $n_{resid} = \bar{n}_{resid}(t)$ in the region $t_{as} < t < t_{exp}$. We estimate the error of $n_{resid}(t)$ as the maximum of its standard deviation and its drift.

It is important to note that, within our experimental time scale, the long-lasting uptake accounts for most of the uptake. About $(5-8) \times 10^{13}$ HCl molecules/cm^2 can be attributed to the initial fast processes, while 5−10 times this amount is taken up onto the ice within 2500 s.

Could Experimental Pitfalls Cause the Residual Component? We can exclude that HCl adsorption on newly exposed glass after opening the plunger significantly contributed to the observed uptake behavior. For HCl uptake experiments on sulfuric acid at similar temperatures, the measured uptake is lower than predicted by the asymptotic model during the initial phase of the experiment. This is consistent with the HCl partial pressure in the cell dropping after the plunger has been opened, which causes the HCl to desorb from the cell walls. Thereby, less HCl is consumed from the regular gas flux leading to a seemingly lower uptake coefficient (cf. eq 20 in Appendix A). This has also been observed by Williams and Golden[86] for the uptake of HCl on sulfuric acid.

The wall effects on the HCl uptake must be equal in sign and similar in magnitude for both the ice and the sulfuric acid experiments. Thus, the enhanced uptake during the initial phase of the HCl uptake must be due to the HCl ice interaction. This argument is corroborated by measurements of Abbatt et al.,[25] who estimated the uptake of HCl on cold glass surfaces on the order of 10^{12} molecules cm^{-2}. When opening the plunger, we expose less than 15 cm^2 new glass surface area, while the ice surface area is about 4.5 cm^2. On the basis of these data, we estimate the maximum error of the measurement due to wall effects as $10^{12} \times 15/4.5 \approx 4 \times 10^{12}$ molecules/cm^2, which is negligible in comparison with the total uptake. We adopt the value of 5×10^{12} molecules/cm^2 or ∼0.5% of an HCl monolayer on the ice as the detection limit of our system.[87]

From the water vapor pressure measurement, we have calculated the net growth and evaporation rate during the experiments as ±300 monolayer during the whole course of the experiments. Assuming a mixing ratio of $x = 10^{-4}$ in the ice, (which is large compared to the overall HCl solubility in ice), the maximum amount of HCl which can be built into a newly grown 300 monolayer thick ice film on top of the ice is small compared to the residual nondiffusive component. Furthermore, it should be noted that in about half of the experiments there was a net evaporation of ice, which precludes additional HCl uptake into a newly grown ice film on the surface. As the residual component was observed in experiments with both growing and evaporating ice, a slight mismatch of the vapor pressure and a net ice growth cannot have caused the residual nondiffusive component.

Langmuir Adsorption and Diffusion. It is tempting to hypothesize that the observed uptake kinetics points toward a two-step uptake process: a slow, long-lasting diffusive uptake process and a fast initial process, possibly adsorption of HCl on the ice surface uptake. In the literature, Langmuir adsorption has been invoked to model the uptake of HCl on ice.[9,10,12,88] In the following, we will test the consistency of this hypothesis with the experimental data.

The residual between total and diffusion-like uptake, which we have calculated in the previous section, allows to assess the order of magnitude of the non-diffusion-like component of the overall uptake. However, this approach does not take the coupling and competition between bulk diffusion and surface adsorption into account. No analytical solution to the quantification of coupled diffusion and surface uptake is available; therefore, we use a numerical model to evaluate the data.

In the numerical model, we assume that the HCl is taken up onto the surface by a Langmuir adsorption kinetics and by diffusion into the bulk ice. The model is detailed in Appendix B. It has two input parameters, $H_d D^{1/2}$ and θ_{equi}, where θ_{equi} is the equilibrium surface coverage on the geometric ice surface at the given HCl partial pressure p_0. We define the units such that $\theta = 1$ corresponds to a surface concentration of 10^{15} molecules/cm^2.

The dashed dotted line in Figure 4 shows the asymptotic fitting (i.e., for $t > 900$ s) of the numerical model with the choice

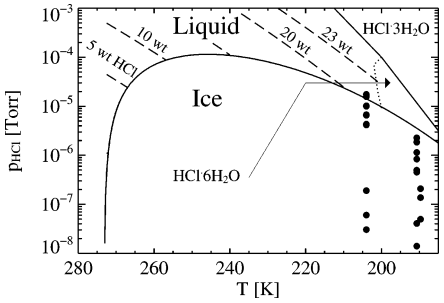

Figure 5. HCl/ice phase diagram, calculated from Carslaw et al.[90] Dotted line: HCl−hexahydrate (taken from Molina[57]). Thick circles mark present work. Dashed lines: HCl mass fraction in the HCl/water solution.

$\theta_{max} = 0$, that is without surface uptake.[89] Clearly, the numerical model coincides well with the analytical equations (eq 23) in absence of surface adsorption.

Now, the two parameters, θ_{equi} and $H_d D^{1/2}$ were fitted simultaneously to the experimental data for the whole time span of the experiment (dashed line in Figure 4b). To avoid experimental artifacts in the analysis, due to a slow opening procedure of the plunger, the first 15 s after opening the plunger were omitted from the fit. The result of this procedure is shown in Figure 4, parts b and c, as dashed lines. The full model describes also the initial part of the signal reasonably well. In the presented case, there is a slight systematic deviation during the initial period of the uptake. We note that Figure 4 represents a case whose fit in the initial period is worse than in most of the other cases. Because the full numerical model predicts a slightly faster saturation than experimentally observed, but a slower approach to the $t^{1/2}$ asymptote, the model will slightly overestimate the contribution of the adsorption to the tailing.

The total uptake in the experiment and the contribution of the diffusion-like and nondiffusive component are plotted in Figure 4d. Interestingly, both the asymptotic model and the full numerical simulation show similar results. The long-term tailing is completely dominated by the diffusion-like component. Thus, surface adsorption with Langmuir type kinetics would only be consistent with the experimental data, if it contributes to the uptake only during the initial stage of the experiment. For practical matters, the two processes are almost completely decoupled.

It was not possible to fit the data using Langmuir kinetics without any diffusive component. As the Langmuir kinetics is essentially first order, it predicts an exponential asymptote, but not the experimentally observed $t^{1/2}$ law.

Pressure Dependence of the Diffusion-Like Uptake. The knowledge of the HCl/water phase diagram is essential to interpret the HCl uptake. Using the thermodynamic model of Carslaw et al.,[90] we calculated the HCl ice phase diagram (Figure 5). The experimental conditions chosen in this study are marked as solid circles in the phase diagram. Most of the experiments have been performed in the ice stability region.

First, we present the results for $H_d^* D^{1/2}$ at 190 and 203 K as a function of the HCl partial pressure in Figure 6. The results for the asymptotic model and the full numerical simulation coincide closely (in most cases better than 20%, cf. Table 1); thus, only the results for the numerical model are shown. The error for $H_d^* D^{1/2}$ was determined from the standard deviation of the nonlinear fitting procedure. For the error of the HCl partial pressure, see the Experimental Section. At both temperatures, $H_d^* D^{1/2}$ decreases with increasing HCl partial pressure. We fitted a function of the form $H_d^* D^{1/2} = ap^b$ to the data and found $-0.55 > b > -0.48$ for 190 and 203 K for both the asymptotic and the numerical model (Table 3 and solid line in Figure 6). The observed proportionality $H_d^* D^{1/2} \propto p^{-0.5}$ would be consistent with the hypothesis that the long-term tailing is indeed caused by the dissolution, dissociation, and diffusion of H^+ and Cl^- into a yet unknown reservoir.

TABLE 1: Results for $H_d^* D^{1/2}$ at 203 K (Upper Panel) and 190 K (Lower Panel) as Determined by Different Methods of Data Analysis (See Text)

p (Torr)	$H_d^* D^{1/2}$(asymptotic) (m s$^{-1/2}$)	$H_d^* D^{1/2}$(numerical) (m s$^{-1/2}$)
	203 K	
3×10^{-8}	18 ± 4	16 ± 6
6×10^{-8}	16 ± 4	15 ± 6
9.4×10^{-8}	10.3 ± 3	7.5 ± 6.7
1.9×10^{-7}	6.3 ± 0.5	5.8 ± 2
2.5×10^{-7}	4.2 ± 1	3.1 ± 0.8
4.9×10^{-7}	4.0 ± 0.7	4.0 ± 1
4.2×10^{-6}	1.3 ± 0.3	1.5 ± 0.3
4.3×10^{-6}	1.3 ± 0.4	1.5 ± 0.9
6.6×10^{-6}	0.85 ± 0.1	0.83 ± 0.4
6.7×10^{-6}	0.93 ± 0.4	1.0 ± 0.2
1×10^{-5}	0.86 ± 0.3	1.4 ± 0.9
1×10^{-5}	0.8 ± 0.1	0.86 ± 0.2
1.6×10^{-5}	1.24 ± 0.08	1.24
1.7×10^{-5}	1.43 ± 0.1	1.16 ± 0.2
	190 K	
4.9×10^{-8}	13 ± 2	11 ± 5
1.4×10^{-7}	12 ± 3	10 ± 3
2.1×10^{-7}	15.6 ± 0.5	13 ± 2
1.4×10^{-8}	23 ± 6	22 ± 43
4.1×10^{-8}	19 ± 4	17 ± 9
4.5×10^{-7}	2.5 ± 0.5	3.0 ± 1
5.0×10^{-7}	3.2 ± 1	3.4 ± 3
8.3×10^{-7}	3.4 ± 0.3	3.0 ± 0.8
1.1×10^{-6}	2.1 ± 0.6	1.8 ± 0.5
2.3×10^{-6}	2.3 ± 0.2	2.3 ± 0.6
1.9×10^{-6}	1.8 ± 0.3	2.1 ± 1.1

Properties of the Nondiffusive Component. In Figure 7, we show the residual component n_{resid} as calculated from the asymptotic fitting method, θ_{equi} as derived from the numerical model, and $n_{2/3}$ as derived from the two-third model. The two-third model ignores all uptake for times after signal recovery to two-thirds of its original value, ignoring the time dependence of the uptake process. Open circles show the total HCl uptake $n_{exp}(t = 1800\ s)$ after 1800 s calculated by numerical integration of the signal with eq 25 (see Appendix A). It must be emphasized that the majority of the overall uptake can be explained with a diffusive kinetics. For the 203 K data, within the first 1800 s typically 80% (50% for the 190 K data) of the overall uptake can be explained with diffusion-like kinetics (open circles in Figure 7; see also Table 2). Thus, the residual component is a minor contribution to the overall HCl uptake.

We estimate that the nondiffusive component is on the order of 1−10% of a monolayer coverage. The order of magnitude of the nondiffusive component is consistent with the result from Chu[27] (open diamond in Figure 7), who estimated an surface uptake of 2×10^{13} molecules/cm^2 at 188 K and 2.1×10^{-7} Torr, by accounting for the porosity of the ice films in a flow tube study.

The total uptake (open circles in Figure 7) shows a clear pressure dependence: $n_{tot} \propto p^{1/2}$. The pressure dependence of the residual component is less clear. At 203 K, the result from the numerical model, θ_{equi}, and the residual from the asymptotic method, θ_{resid}, roughly follows a $p^{1/2}$ law. In contrast, evaluation with the two-thirds method shows a weaker pressure dependence.

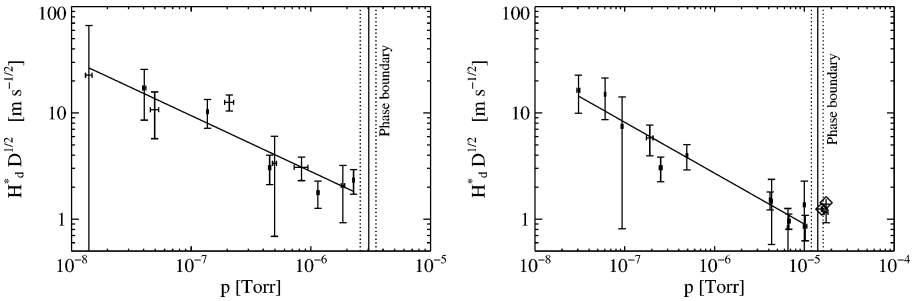

Figure 6. Results for $H^*_dD^{1/2}$, as evaluated with the numerical model at 190 K (left panel) and 203 K (right panel): diamonds: estimate with asymptotic model in melting regime; vertical solid line: ice−liquid phase boundary as calculated from Carslaw et al.;[90] dotted lines: uncertainty of the phase boundary position due to absolute error of the pressure measurement; solid line: fit to the data with relation $H^*_dD^{1/2} = ap^b_{0,exp}$ (cp. Table 1).

TABLE 2: HCl Uptake on Ice as Determined by Different Data Evaluation Methods at 203 K (Upper Panel) and 190 K (Lower Panel)[a]

p_0 (Torr)	t_{exp} (s)	hole	θ_{tot}	θ_{resid}(asymptotic)	θ_{equi}(numerical)	$\theta_{2/3}$
			203 K			
3.0×10^{-8}	5886	5	0.13	0.012 ± 0.001	0.01 ± 0.03	0.030
6.0×10^{-8}	5414	5	0.23	0.015 ± 0.002	0.006 ± 0.04	0.043
9.4×10^{-8}	787	4	0.043	0.0012 ± 0.0006	0.006 ± 0.09	%[b]
1.9×10^{-7}	1606	5	0.15	0.022 ± 0.0006	0.026 ± 0.023	0.044
2.5×10^{-7}	547	4	0.053	0.0053 ± 0.002	0.017 ± 0.03	0.043
4.9×10^{-7}	4281	5	0.57	0.085 ± 0.004	0.035 ± 0.035	0.060
4.2×10^{-6}	699	5	0.54	0.13 ± 0.002	0.07 ± 0.06	0.078
4.3×10^{-6}	3349	5	1.63	0.33 ± 0.01	0.13 ± 0.1	0.11
6.6×10^{-6}	3031	5	1.2	0.32 ± 0.009	0.18 ± 0.15	0.095
6.7×10^{-6}	2732	5	1.3	0.25 ± 0.03	0.15 ± 0.09	0.11
1.0×10^{-5}	2296	5	1.7	0.27 ± 0.03	0.073 ± 0.8	0.11
1.0×10^{-5}	2444	4	1.6	0.26 ± 0.01	0.087 ± 0.1	0.17
1.6×10^{-5}	3943	4	4.2	%[c]	%[c]	0.27
1.7×10^{-5}	3346	4	4.8	%[c]	%[c]	0.21
			190 K			
5.0×10^{-8}	738	5	0.042	0.0052 ± 0.0003	0.008 ± 0.02	0.029
1.4×10^{-7}	392	4	0.10	0.035 ± 0.0006	0.046 ± 0.02	0.049
2.1×10^{-7}	2708	5	0.47	0.055 ± 0.0009	0.1 ± 0.08	0.21
1.4×10^{-8}	2461	6	0.046	0.019 ± 0.0005	0.26 ± 0.07	0.029
4.1×10^{-8}	5961	5	0.17	0.043 ± 0.001	0.047 ± 0.06	0.082
4.5×10^{-7}	4181	4	0.35	0.11 ± 0.001	0.037 ± 0.05	0.12
5.0×10^{-7}	1074	6	0.18	0.079 ± 0.003	0.085 ± 0.053	0.076
8.3×10^{-7}	1814	4	0.34	0.0096 ± 0.002	0.009 ± 0.06	0.12
1.1×10^{-6}	310	6	0.11	0.078 ± 0.005	0.11 ± 0.06	%[b]
2.3×10^{-6}	7175	4	1.51	0.13 ± 0.01	0.064 ± 0.1	0.24
1.9×10^{-6}	5376	4	1.3	0.25 ± 0.003	0.075 ± 0.15	0.21

[a] p_0: HCl partial pressure when plunger closed; t_{exp}: duration of experiment; hole: used position of hole to mass spectrometer, see text; θ_{tot}: total measured uptake; θ_{resid}: nondiffusive residual as determined with asymptotic model; θ_{equi}: surface uptake with numerical model; $\theta_{2/3}$: uptake with two-thirds model. [b] Signal did not rise to two-thirds value, as the experimental time scale was to short. [c] No residual was detectable, and the initial uptake was less than predicted by a diffusive model, when the HCl partial pressure is high enough to melt ice.

TABLE 3: Parametrization of HCl Uptake by Different Models[a]

method	T [K]	a	b	c	d
asymptotic	203	-2.838 ± 0.4	-0.55 ± 0.06	17.73 ± 1.7	0.6556 ± 0.3
asymptotic	190/188	-2.860 ± 1.4	-0.55 ± 0.2	16.40 ± 3.4	0.4177 ± 0.2
numerical	203	-2.440 ± 0.7	-0.479 ± 0.1	16.763 ± 1.3	0.5279 ± 0.2
numerical	190/188	-2.709 ± 1.2	-0.5263 ± 0.2	14.99 ± 1.3	0.1862 ± 1.1
two-third	203	n/a	n/a	15.55 ± 0.6	0.28 ± 0.1
two-third	190/188	n/a	n/a	16.5 ± 1.6	0.4 ± 0.3

[a] Parameters are given to calculate diffusion parameters and surface uptake by $H^*_dD^{1/2} = 10^a \times p^b$ and $n_{surf} = 10^c \times p^d$, respectively. The pressure p is given in units of Torr; $H^*_dD^{1/2}$ is in units of cm s$^{-1/2}$. Note that the fits were performed as linear fits in a logarithmic scale: $\log[H_dD^{1/2}] = a + b \times \log_{10}p$ and $\log_{10}[N_{surf}] = c + d \times \log_{10}p$. Numbers given in this table contain more digits than are significant, to allow reproduction of the parametrization plotted into Figures 9 and 10.

We cannot make a definite claim about the nature of the residual component, but we can test the compatibility with models for the adsorption isotherm, as demonstrated in Figure 7. For both 203 and 190 K, a Langmuir type isotherm for a dissociating species ($\theta(p) = \text{const} \times (ap)^{1/2}/(1 + (ap)^{1/2})$ see Trapnell[91]) can be fitted to the experimental data. However, the Langmuir adsorption isotherm for a nondissociating species ($\theta(p) = \theta_{max} \times p/(K + p)$) would also fit, if one assumed the limiting coverage to be lower than 10^{15} molecules/cm^2 (cf. Figure 7). We suggest that at present an adsorption isotherm cannot be reliable established for the HCl uptake on ice. To the best of our knowledge, there are no other studies available

TABLE 4: HCl Uptake on Ice from Previous Studies[a]

author		T (K)	P (10^{-6} Torr)	uptake (10^{15}/cm^2)	expt time scale (min)	ice type	ice thickness (μm)
Abbatt et al.[25]	FT	201	1−4	1−3	5−35	vp	5−40
Barone et al. [23]	KN	202	5	3.5	30−60	vp	0.051
Chu et al.[27]	FT	188, 193	0.07−4	0.1−0.2	15−90	vp	1.4 ± 0.2
	FT	188	0.02	0.02[b]		vp	0.5−15.7
Chu[27]	FT	188	not given	0.8−11		vp	3.7−34.1
Foster[29]	LITD	180−186	0.001−0.6	0.4−20[c]	%	vp	%
			%	1.15[d]	%		%
Hanson and Ravishankara[26]	FT	201	0.04−1.5×	0.4−0.6[e]	varies	vp	3−30
		201	0.2	0.5	5	vp	%
Hynes[30]	FT	205	0.4−2	∼0.2	∼5	s	%
		205−230	1.2	∼0.3−0.1	%	s	%
Lee[92]	TFT	201	0.15−4	0.1−0.4	%	s	%
		201	2	∼0.3	%	vp	%

[a] Abbreviations: FT: flow tube; KN: Knudsen cell; TFT: turbulent flow tube; LITD: laser-induced thermal desorption; vp: vapor-deposited ice; s: smooth ice film, grown from distilled water. [b] Data point derived using the internal surface area of the ice film. [c] Data vary with ice preparation time. [d] For smooth ice film. [e] Observed uptake varies by a factor of 2 with thickness.[32,33]

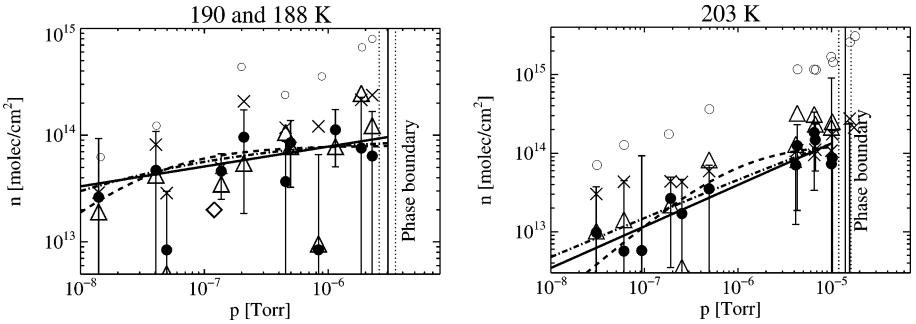

Figure 7. Total uptake and nondiffusive component of uptake. Left panel: 188 K and 190 K. Right panel: 203 K. Key: open circles: total uptake at $t_{norm} = 1800$ s; crosses: uptake calculated from the two-thirds method; open triangles: residual uptake n_{resid} as calculated from the asymptotic model; filled circles: surface adsorption $n_{resid} = \theta_{equi} \times 10^{15}$ molecules/cm^2 as calculated from numerical model; solid line: fitted Freundlich isotherm for surface uptake (cp. Table 3); dashed line: fitted Langmuir type isotherm ($\theta_{resid} = \theta_{max}p/(\tilde{K} + p)$, fit parameter θ_{max} and $\tilde{K}$) with $\theta_{max} = 0.13$, $\tilde{K} = 1.02 \times 10^{-6}$ Torr for 203 K and $\theta_{max} = 0.079$, $\tilde{K} = 3.23 \times 10^{-8}$ Torr for 190 K; dashed-dotted line. fitted Langmuir isotherm for a dissociating species ($\theta_{resid} = \theta^*_{max}\sqrt{K'p}/(1 + \sqrt{K'p})$, fit parameter θ_{max} and K') e.g. p 111, in ref 91), with $\theta_{max} = 1$, $K' = 2304$ Torr^{-1} for 203 K, and $\theta_{max} = 0.0946$, $K' = 2.157 \times 10^7$ Torr^{-1}, for 190/188 K (note that points with $n < 10^{13}$ molecules cm^{-2} were excluded from the fit); open diamond: surface uptake as measured by Chu et al.[27] estimated using a porosity model. Note that there was no measurable residual uptake for HCl pressures high enough to melt the ice.

which could resolve this fundamental problem. Thus, for simplicity we use the Freundlich isotherm[77] ($n_{surf} = ap_0^b$), as derived from the asymptotic model for parametrization.

HCl Uptake on Previously Exposed Ice. At 203 K, we also performed uptake experiments on ice that had been previously exposed to HCl. One example is shown in Figure 8. Repeated exposure typically shows diffusive kinetics according to eq 9 (center panel of Figure 8). However, in distinct opposition to experiments on fresh ice (cf. Figure 4), no enhanced initial uptake was observed.

Clearly, the ice surface was changed by the first exposure and becomes less susceptible to gaseous HCl. Compared to experiments on clean ice, $H^*_dD^{1/2}$ is slightly reduced (due to some HCl already present), but still shows the same principal partial pressure dependence, i.e., increasing $H^*_dD^{1/2}$ with decreasing HCl partial pressure (not shown). This observation is in agreement with a diffusive uptake process.

The experimentally observed fact that the initial high HCl uptake vanishes upon second exposure, while the long-term tailing still follows a $t^{1/2}$ kinetics, further corroborates the hypothesis that the initial fast uptake and the long tailing are indeed two different physical processes.

HCl Uptake at High HCl Partial Pressures. The principal uptake behavior changes drastically, if the HCl partial pressure is high enough to melt the ice. However, even then the kinetics is diffusive. But now $H^*_dD^{1/2}$ rises with partial pressure, indicating that the ice surface melts faster for higher HCl partial pressures. Most importantly, no fast initial uptake process can be detected experimentally. Again, this observation support the notion that the diffusive kinetics and the initial enhanced uptake are caused by two distinguishable and largely decoupled physical processes.

Semiempirical Parametrization of the HCl Uptake. Solely based on our experimental observations, we formulate a semiempirical parametrization for the HCl uptake on vapor-deposited ice. The parametrization reflects our two main experimental observations: First, the overall long-term uptake is slow and follows a $t^{1/2}$ law, as demonstrated in Figure 4d. Second, the long-term uptake follows a $p^{1/2}$ law. Thus, the total HCl uptake must be given as a function of time and partial pressure, instead of simply giving a result in terms of uptake per surface area. A reasonable parametrization should have the general form

$$n_{tot}(t) = n_{resid}(p) + C(T)\sqrt{tp_{HCl}} \tag{10}$$

where the term $n_{resid}(p)$ accounts for the part of the uptake, which cannot be described by the $t^{1/2}$ law. For practical matters, we can use the results in Table 3 and eq 11 total to parametrize the total HCl uptake as

$$n_{tot}(t) = \text{const} \times p^d + 2H^*_d\sqrt{D}\,\frac{p}{k_BT}\sqrt{\frac{t}{\pi}} \tag{11}$$

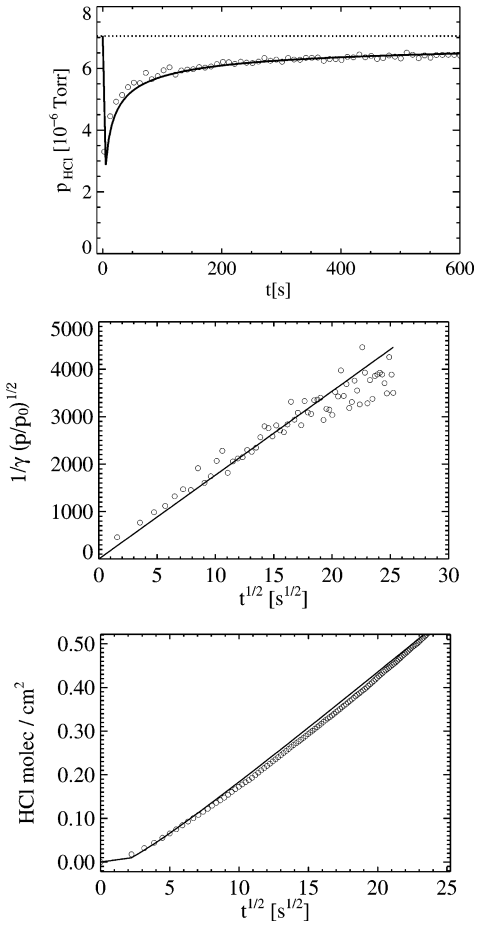

Figure 8. Upper panel: HCl uptake experiment on previously exposed ice. Key: open circles: measured data; solid line: curve calculated from fit in center panel; dotted line: HCl concentration with plunger closed (p_0). Center panel: uptake coefficient as a function of $t^{1/2}$. Key: open circles: measured data; solid line: fit according to eq 9. Lower panel: total uptake as a function of time. Key: open circles: calculated by numerical integration of the measured data; solid line: calculated from simulated HCl partial pressures (both eq 25).

Comparison with Other Studies. A tailing of the signal has been observed in many previous studies. For example, Chu et al.[27] found more pronounced tailing when increasing the film thickness. For HNO_3 a diffusive kinetics has been observed for long time scales.[38] However, incomplete information about the experimental conditions renders direct comparison of total uptake and its kinetics with other laboratory experiments difficult; in particular, information on exposure times is often not provided as it is deemed unimportant.

In Figure 9, we compare our data with the work of Chu et al.,[27] which were obtained on 1.4 μm thick vapor-deposited ice films. These experiments were performed with typical time scales of roughly 30 min. For comparison, we show the total uptake as determined in the present study within 30 min after opening the plunger. Experiments that lasted less than 30 min are not included in the plot. The three data sets coincide well in the amount of uptake and its dependence on HCl partial pressure. The lines show the parametrization of the HCl uptake (eq 11) based on the both the asymptotic and the numerical model for various experimental time scales (see caption). For completeness, we note that Flückiger and Rossi[24] (not shown) investigated the very first few seconds of the HCl uptake on ice and derived a factor of 5 less uptake than estimated by the asymptotic model for pressures below 2×10^{-6} Torr, while

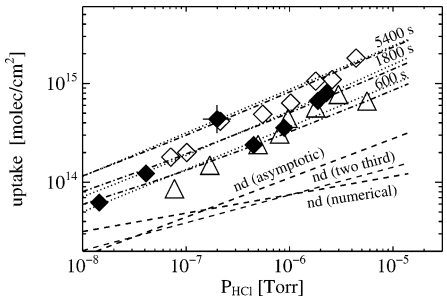

Figure 9. Comparison of total HCl uptake on vapor-deposited ice at temperatures around 190 K; solid diamonds: this study, calculated by numerical integration to $t = 30$ min, as typical for the experimental exposure times applied by Chu et al.[27] Solid diamond with cross: data at 188 K; open triangles and diamonds: from Chu et al.[27] at 193 and 188 K, respectively (note that the data points at highest pressures are not in the ice stability regime); dotted lines: parametrization of HCl uptake according eq 11 for $t = 600$, 1800, and 5400 s, as calculated from the asymptotic model; dashed−dotted lines: parametrization of HCl uptake according to eq 11 for $t = 600$, 1800, and 5400 s, as calculated using the numerical model; dashed lines: estimated non-diffusive contribution n_{resid} from different models calculated using eq 11.

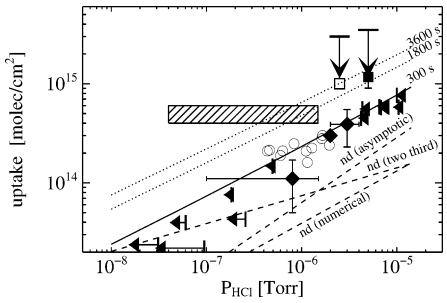

Figure 10. Comparison of total HCl uptake on ice at temperature around 200 K. Open circles: Hynes et al.[30] at 205 K; hatched area: Hanson and Ravishankara;[26] filled diamonds: Lee et al.[92] at 201 K, average of several experiments; filled square: Abbatt et al.;[25] open square: Barone et al.[23] at 202 K on crystalline ice; vertical arrows show correction for diffusive kinetics; arrows start at original data $n(t_{exp})$, and the tips of arrows point toward time corrected points $n(t = 300\ s) = n(t_{exp}) \times (t_{norm}/t)^{1/2}$; horizontal arrows: this study, total integrated uptake after 300 s; end of arrow marks p_0; tip of arrow marks p_r after 300 s; solid line: parametrization based on asymptotic model with eq 11 for $t_{norm} = 300$ s; dotted lines: estimated HCl uptake after 1800 and 3600 s from eq 11, respectively; dashed lines: nondiffusive components calculated from several models using parameters from Table 3 and eq 11.

they estimated strongly rising uptake for HCl partial pressures very close to the ice melting point.

The HCl uptake from various other studies at temperatures around 200 K is compared in Figure 10. We show the total integrated uptake of the present study at $t_{norm} = 300$ s to facilitate comparison with the data from Hynes et al.[30] The time $t_{norm} = 300$ s is short compared to the recovery time of the HCl partial pressure in our experiments. The recovery time of the signal is mainly a feature of the design of the specific flow-tube or Knudsen cell. However, close to saturation on the surface, when the diffusive transport dominates, the total uptake is only a function of time,[44] that is, $n_{tot}(t) = 2H_d^*\sqrt{D}\sqrt{t/\pi}\ p/(k_B T)$. The partial pressure drop from p_0 to p_r at time t_{norm} is symbolized by horizontal arrows, their tip pointing to $p_r(t_{norm})$. Because the signal has not yet recovered, the uptake has been performed at partial pressures $p < p_r(t_{norm})$ and not at p_0. Thus, the tips of the arrows are more appropriate representations of the HCl partial pressures during the uptake than p_0. The dotted lines

show the estimated HCl uptake for 1800 and 3600 s, respectively. These lines demonstrate the impact of diffusion-like kinetics on uptake processes. They point toward possible pitfalls when deriving the uptake of acidic gases solely from the total uptake without using proper microphysical modeling or taking changes of the partial pressure in the reactor into account.

In Figure 10, open circles are taken from Hynes et al.,[30] who used the "two-thirds" criterion[38] to determine the total HCl uptake in a flow tube experiment on smooth ice films. The duration of these experiments cannot easily be inferred, however, based on Figure 1 in Hynes et al.,[30] the time scale might be roughly 300 s. With this assumption, the magnitude of uptake measured in our experiments coincides very well with with the work of Hynes et al.[30] However, the data from Hynes et al. show a weaker pressure dependence. Our data further agree within experimental error with the pressure dependence of the data from Lee et al.[92] (filled diamonds), allthough the absolute values cannot be compared as the exposure time of this experiment is not known.

The hatched area in Figure 10 shows the range of data as reported by Hanson and Ravishankara.[26] These authors observed a reversible and an irreversible component of the HCl uptake, which were attributed to surface uptake and dissolution respectively.[93] On the basis of a HCl solubility limit of 20 ppmv in ice[94] and a diffusion constant of 10^{-11} cm^2 s^{-1}, Hanson and Ravishankara estimated the contribution of dissolution to the overall signal as less than 10%. The time scale of their uptake experiment at 2×10^{-7} Torr is about 5 min, as in the other data in the figure. This measured uptake at 2×10^{-7} Torr is about a factor of 4 higher compared to other studies and our parametrization. Interestingly, the uptake in this study is reported to be independent of the HCl partial pressure (hatched area in Figure 10).

Data from the early work of Abbatt et al.[25] are also shown in Figure 10. The filled square show the data scaled to experimental duration of 300 s using a $t^{1/2}$ law. This is illustrated by a vertical arrow pointing toward the open square. The arrow starts at the original data point ($n_{tot}(t_{exp} = 2100\ s) = 3 \times 10^{15}$ cm^2) and points toward the scaled value of $n_{tot}(t_{norm}) = n_{tot}(t_{exp} = 2100\ s)(t_{norm}/t_{exp})^{1/2}$. Similarly, we treated the data from Barone et al.[23] (arrow pointing to the open square). Again, the arrow starts at the original data point and points toward its value after scaling with $t^{1/2}$ kinetics.

The data from Abbatt at al.[25] and Barone et al.[23] are brought into much better agreement with our parametrization of the HCl uptake and the data of Hynes and Hanson and Ravishankara by assuming a $t^{1/2}$ kinetics using our parametrization of the HCl uptake. However, an unexplained discrepancy of a factor of 4 remains. It is suspected that morphological differences or other experimental factors may cause the remaining difference.

In Figures 9 and 10, we plot the nondiffusive component (dashed lines), as estimated from the asymptotic and numerical model, and also the result from the data evaluation using the two-thirds method. For both temperatures, the magnitude of nondiffusive uptake obtained by these methods is comparable, while the results for the pressure dependence remain highly uncertain (with slopes 0.3−0.6). As the nature of the uptake process is not well understood, we cannot claim that the applied data evaluation methods reflect the physical uptake on the ice surface itself. Rather we use the nondiffusive component to make the point that in absence of a clear understanding of the nature of the uptake process, care must be taken when analyzing uptake experiments and defining criteria to determine the HCl uptake per surface area.

Summary and Discussion

In this work, we investigate the HCl uptake on vapor-deposited ice films. Main result of our experiments is that the uptake of HCl is governed by a slow, long-lasting uptake process with a diffusion-like kinetics $n_{tot}(t) \propto t^{1/2}$. The analysis of the long-term uptake in terms of a diffusive model shows that the tailing can be described by **one single quantity**, $H_d^* D^{1/2}$, which exhibits a distinct pressure dependence: $H_d^* D^{1/2} \propto p^{1/2}$, as expected for a diffusing, dissociating species. While the major part of the overall uptake can be accounted for by a diffusion-like kinetics (e.g., 4), for the initial period of the uptake process the uptake is higher than compatible with diffusion-like kinetics. Furthermore, data show that the major part of the overall uptake n_{tot} can be accounted for by diffusion-like kinetics, as demonstrated in Figure 4c.

Similarly, diffusive kinetics with a $H_d^* D^{1/2} \propto p^{1/2}$ dependence, (but without the sensitivity to detect the possibly enhanced initial uptake) has been found for the uptake of SO_2 into packed ice beds[44] for temperatures between −30 and 0 °C. Thus, this behavior might be a general feature for the uptake of acidic trace gases on ice. In contrast, for SO_2 uptake experiments in a flow tube experiment at temperatures around 200 K no tailing was observed.[95] However, as the SO_2 uptake in these experiments was very low, one might speculate whether any tailing would have been detectable in a flow tube experiment with a surface which is small compared to the packed ice bed experiments.

On the basis of experimental observations, it is tempting to speculate that there are basically two physical processes responsible for the uptake of HCl on ice: uptake on the physical surface area and concurrent and subsequent diffusion into a yet unknown reservoir. Also, it should be emphasized that to the best of our knowledge the existence of a simple adsorption process on the surface has not yet been established by direct experimental evidence. Furthermore, the influence of the ice porosity on the trace gas uptake remains controversial in the literature.[32−33,96] In the following, we will discuss several conceivable uptake processes and possible reservoirs and the compatibility with the experimental observation.

Surface Adsorption. Monolayer adsorption has been invoked to describe the HCl adsorption on ice.[9,10,12] To assess the possibility of monolayer adsorption, we estimate the maximum possible surface uptake. Solely based on geometric considerations (i.e., the diameter of the Cl^- ion of about 3.6 Å, based on the ion size in a sulfuric acid solution[97]) about $n_{HCl,surf} = 7.8 \times 10^{14}$ HCl molecules/cm^2 form a monolayer on a smooth surface. This upper limit would be consistent with the measured residual uptake n_{resid}, if it is interpreted as uptake on the geometric ice surface itself. However, we have observed a total uptake of more than one monolayer at high HCl partial pressures. Thus, to describe the overall uptake, the physical picture of a monolayer adsorption can only be possible if the physical surface area is much higher than the geometric one, as it is the case for porous or very rough ice.

Diffusion into the Ice and Its Crystal Matrix. The diffusion of HCl in ice at temperatures around 200 K has been investigated by various authors using diverse techniques. These data scatter widely (Table 5). The value of 10^{-16} m^2 s^{-1} seems a reasonable upper limit for the diffusion of HCl into ice at temperature around 200 K.[98] Then, for typical experimental time scales of 30 min, the diffusion depth $\Delta x = (Dt)^{1/2}$ is less than 1 μm, which is smaller than the thickness of the ice films used in our experiments. Thus, diffusion will occur in the upper part of the bulk ice.

TABLE 5: Available Data on Diffusion Constants for HCl in Ice

author	T (K)	D (m^2 s^{-1})	comment
Barnaal and Slotfeldt-Ellingsen[119]	258	4×10^{-13}	NMR, frozen doped solution
Dominé et al.[120]	258−268	$(2.6-38) \times 10^{-16}$	single crystal
	190	3.6×10^{-22} to 1.3×10^{-20}	extrapolated
Flückinger et al.[22]	190−200	$(4 \pm 0.1) \times 10^{-18}$	single-crystal
		5.6×10^{-17} to 2.8×10^{-16}	polycrystalline
Huthwelker et al.[121]	203	$(1-4) \times 10^{-17}$	bulk ice, RBS
Krishanan and Salomon[14]	255−269	4.9×10^{-12} to 1.6×10^{-11}	diffusion at the HCl/ice phase boundary
Krieger et al.[110]	195	5×10^{-16} to 3×10^{-15}	RBS, frozen doped solution
Molina et al.[122]	185	10^{-13}	vapor grown ice, under melting conditions[25]
Thibert and Dominé[19]	265−238	10^{-16} to 10^{-15}	single crystal
Wolff et al.[69]	185 and 253	10^{-14} and 10^{-17}	values are upper limit only

TABLE 6: Symbols Used

symbol	meaning	units
γ	uptake coeff	
D	diffusion constant	m^2 s^{-1}
H	Henry's law constant	mol L^{-1} atm^{-1}
H_d	dimensionless Henry's law constant	
H_d^*	effective dimensionless Henry's law constant	
j	flux density	m^{-2} s^{-1}
k_B	Boltzmann constant	
k	dissociation constant	m^3
m	molecular mass	kg
n_g	concentration in the gas phase	m^{-3}
n_i	concentration in the ice	m^{-3}
n_{resid}	residual, nondiffusive	m^{-2}
n_{surf}	surface concentration	m^{-2}
n_{sites}	no. of available sites	m^{-2}
n_{tot}	total uptake	m^{-2}
N_c	no. of molecules in cell	
p	pressure	Pa, Torr
p_c	pressure in Knudsen cell	Pa, Torr
p_0	partial pressure in Knudsen cell with closed plunger	Pa, Torr
p_r	partial pressure in Knudsen cell with open plunger	Pa, Torr
p_v	vapor pressure	Pa, Torr
R	rate	s^{-1}
R_0	rate of molecules into Knudsen cell	s^{-1}
R_{MS}	rate of molecules into mass spectrometer	s^{-1}
R_S	rate of molecules on substrate	s^{-1}
t	time	s
t_{exp}	duration of uptake experiment	s
t_{as}	time, when asymptotic fitting starts	s
T	temperature	K
T_S	substrate temperature	K
T_c	wall temperature in Knudsen cell	K
θ	surface coverage	
θ_{equi}	surface coverage, as derived from the numerical model	
θ_{resid}	residual, nondiffusive component of surface coverage	
$\bar{v}$	mean thermal velocity	m/s

On the basis of solubility measurements in ice single crystals at temperatures between 238 and 265 K,[20] the mixing ratio of HCl in the ice is about 10^{-5} at 200 K and 5×10^{-8} Torr of HCl. If we assume that the physical ice surface area is 20 times larger than the geometric surface area[28,32] and that the diffusion depth is about 1 μm along the porous surface, only about $(2-8) \times 10^{12}$ HCl molecules/cm^2 per geometric surface area could dissolve based on the solid-phase solubilty. This amount is too small to explain the total observed HCl uptake.

The observed pressure dependence $H_d D^{1/2} \propto p^{-1/2}$ gives further insight. Thibert and Dominé[19] showed experimentally that the solubility of HCl in ice single crystals follows a $H_d \propto p^{-1/2.73}$ dependency. This is consistent with the thermodynamic argument that the production of defects in the ice matrix will cause the relation $H_d^* \propto p^{-1/3}$, which has been confirmed experimentally.[15] In the present study, we observe a pronounced proportionality of $H_d^* D^{1/2} \propto p^{-1/2}$ with the HCl partial pressure, which contradicts the diffusion into the ice crystal matrix as a dominant uptake process.

Diffusion into Pores. Most of the surface area in porous ice is hidden and is not directly accessible for trace gas molecules impinging on the ice surface. Pores in vapor-deposited ice have typical dimensions in the micrometer range;[32,33] i.e., they are smaller than the mean free path and the transport into the pores can only happen via Knudsen diffusion[99] in the gas phase[96] or by surface diffusion on the ice surface. Whatever the transport process is, the transport into hidden pores could possibly cause a tailing with diffusive kinetics as (see for example ref 100).

We compare the surface uptake with the work of Chu et al.,[27] who demonstrated the dependence of the total uptake on the film thickness and showed stronger tailing of the breakthrough curves with increasing ice thickness (cf. their Figure 2 in ref 27). Leu et al.[28] suggested that the ice surface area increases with the ice film thickness by up to a factor of 8−10[28] and also showed increasing HCl uptake with increasing thickness. This issue is subject to controversy[26,32−34,96] as only very little impact of the film thickness on the HCl uptake was reported by Hanson and Ravishakara,[26] who also argued that the granule size in porous films is independent from the film thickness for very thin ice films.[35] On the basis of BET determinations of the ice surface area and modeling of the thickness dependence of the HCl uptake, Chu found the surface uptake on the order of 2×10^{13} molecules/cm^2 at 188 K and 2.1×10^{-7} Torr. This value is slightly lower than the residual uptake in our measurements (cf. Figure 7), which is consistent with the interpretation that the residual uptake n_{resid} in our study is caused by uptake onto the geometric ice surface which is readily available for uptake, once the plunger is opened.

In summary, the diffusion into the pores of the vapor-deposited ice is a conceivable process, and our results are consistent with several previously published studies.

Diffusion into Interfacial Reservoirs. It has been suggested that interfacial reservoirs, such as the quasi-liquid layer (QLL) on top of the ice surface,[25,56,57,59] grain boundaries and veins (or so-called triple junctions)[44,69] in polycrystalline ice may serve as reservoirs for trace gas uptake. The size of such reservoirs is thermodynamically defined by surface forces, and also by the curvature of the surface (i.e., the Kelvin effect in veins).[65,67,101] In pure ice, the reservoir size increases when approaching the melting point.[45,46,49,50,53,54,102] This would lead to an increasing speed of uptake (i.e., an increase of $H_d^* D^{1/2}$) when approaching the ice melting point by rising the temperature, or alternatively by raising the HCl partial pressure. However, in the present study, no deviation of the proportionality $H_d D^{1/2} \propto p^{-1/2}$ is found when approaching the ice melting point (cf. Figures 5 and 6). Thus, our data indicate that the uptake into grain boundaries or veins is only conceivable if the reservoir size is unaffected by the amount of HCl dissolved (which would not be the case in

pure systems). Only then both a $p^{-1/2}$ pressure dependence and the diffusive-like $t^{1/2}$ kinetics would occur.

Interestingly, for the weak acid SO_2, increasing uptake has been observed when approaching the ice melting point[39,40] in packed ice bed experiments. This has been attributed to size changes of the vein into which the SO_2 diffuses.[44] It is likely that SO_2, which is a weak and much less soluble acid than HCl, has less influence on premelting phenomena. Thus, when SO_2 interacts with interfacial reservoirs the physical properties of the reservoirs (i.e., the temperature dependence of the reservoir size) may dominate the trace gas uptake. In contrast, the strong acid HCl may dominate the physics of the interfacial reservoirs. Indeed, it has been argued that impurities will potentially enhance premelting phenomena[48,103] and increase the reservoir size.

Surface Reconstruction. HCl is a strong adsorbate, which my strongly affect and reconstruct the ice surface.[104−107] Such effects have also been observed for the SO_2 system at cryogenic temperatures,[108] where slow and long-lasting uptake processes have been observed. As HCl is a strong adsorbate, it must be expected that it will affect the nature of the ice surface itself. If such processes started on the surface and slowly penetrated into the bulk ice one may speculate that the kinetics of the reconstruction (and the associated uptake) could be diffusion-like, as observed in our experiments. If so, H_d would be the HCl solubility in the reconstructed region and D would characterize the speed of reconstruction. Such processes might be equivalent to the formation of a QLL by the presence of the gaseous HCl.

Data Evaluation. The nature of the HCl uptake on ice cannot be resolved from uptake experiments without further analysis of the solid phase alone. We do not claim that our results, which are made on vapor deposited and possible porous ice, will be quantitatively equal on smooth ice films. However, we suggest that the principal features, such as the experimental fact that the tailing follows diffusion-like $t^{1/2}$ kinetics, qualitatively apply to rough (porous) as well as smooth ice films, where a diffusion-like tailing and fast initial uptake has been observed as well (ref 38 and to a lower extent also ref 30). Thus, we conclude that the question of how to treat the tailing in the data evaluation is of universal importance.

With the asymptotic model, we propose a novel data evaluation concept for systems with a diffusion-like kinetics, which allows to separate diffusion-like and nondiffusive processes by analysis of the uptake kinetics. Comparison of the asymptotic model with a complete numerical modeling shows that results derived with both models coincide within experimental error (cf. Figure 7, Tables 1 and 2), i.e., both processes dominate in different regimes.

We would like to stress that uptake with diffusion-like kinetics potentially remains experimentally undetected, although it may dominate the overall amount of uptake. Because a diffusion-like uptake coefficient follows the kinetic law $\gamma(t) \propto t^{-1/2}$, which lead to infinite total uptake $N_{tot} \propto \int_0^\infty \gamma(t')\,dt' \sim t^{1/2}$, (of course only until the reservoir as such is filled). In contrast, first-order uptake processes, such as adsorption, obey an exponential time law, $\gamma(t) \propto e^{-\lambda t}$, which results in a finite total uptake: $N \propto \int_0^\infty \gamma(t')\,dt' = 1/\lambda$. Consequently, there is comparably more uptake during the tailing in a system with a $t^{1/2}$ kinetics compared to systems with exponential decay. Thus, for the same instrument sensitivity, relatively more uptake is "lost" in systems with diffusion-like kinetics.[44]

Concluding Remarks. In this study, we found that HCl uptake is dominated by long-lasting diffusion-like kinetics, while during some initial minutes the uptake is higher than predicted by a diffusion-like kinetics. This picture is consistent with a coupled adsorption-diffusion kinetics.

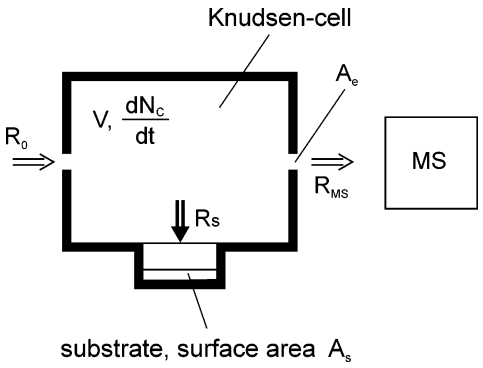

Figure 11. Flux balance in the Knudsen cell. Key: R_0: reflux into the cell; R_{MS}: reflux into the mass spectrometer; R_S: flux onto the substrate.

We suggest the use of a semiempirical formulation to parametrize the time-dependent HCl uptake on vapor-deposited ice by eq 11 with parameters given in Table 3. Reinterpretation of previous studies, which to date have scattered widely, reveals much better agreement using the semiempirical parametrization of the HCl uptake. Consequently, when estimating the HCl uptake on natural ice, the lifetime of the ice or its contact time with the HCl vapor should be considered in eq 11 to calculate the HCl uptake in atmospheric or climate models. A quantification of surface and bulk contributions and the influence of the ice porosity appears to be essential for the understanding of chemical reactions on ice surfaces. Reactions could occur on top of the surface, in the near-surface region, and also in the bulk polycrystalline ice.

Generally, it is difficult to decipher the elemental physicochemical uptake processes of the trace gas uptake onto ice simply by only analyzing the uptake kinetics, as the kinetics delivers no information about the surface itself. From our analysis, simple, noncomposite processes, such as the diffusion into the ice crystal matrix (magnitude of uptake) or a mere Langmuir-type adsorption (uptake kinetics), can be ruled out. Also, diffusion into an existing, by HCl unaffected, QLL appears to be improbable. Conceivable processes are the diffusion into porous ice and the reconstruction of the surface by the presence of the HCl. The latter process might be considered as the induction of a premelt layer by the gaseous HCl.

The determination of elemental concentration profiles in the surface region could provide key data to answer these questions, and effectively improve the analysis of kinetic experiments. Very recently destructive[109] and nondestructive[110,111] methods have been developed to measure concentration profiles in the near-surface region of ice. We suggest that such direct investigation of the ice surface in combination with detailed theoretical analysis of experimental data may provide further necessary insight into physicochemical uptake processes of trace gases on ice.

Appendix A: Kinetics in the Knudsen Cell

Flow Equations in the Knudsen Cell. Figure 11 illustrates the flow conditions in the Knudsen cell. The rate of molecules flowing into the cell is denoted by R_0. Substrate and pinhole to the mass spectrometer act as sinks (rates R_S and R_{MS}, respectively; N_c is the number of molecules in the Knudsen cell). The continuity equation for the cell

$$\frac{dN_c}{dt} = R_0(t) - R_S(t) - R_{MS}(t) \qquad (12)$$

reads in the quasistationary case (i.e., for $R_0 - R_{MS} \gg dN_c/dt$)

$$R_S = R_0 - R_{MS} \tag{13}$$

The flux R_{MS} is calculated from the partial pressure p_c, once the aperture area of the pinhole, A_e, to the mass spectrometer is known (cf. eq 6).

$$R_{MS} = \frac{A_e p_c}{\sqrt{2\pi m k_B T}} \equiv k_e N_c = k_e \frac{p_c V}{k_B T} \tag{14}$$

Using the ideal gas law ($p_c V_c = N_c k_B T$), this equation defines the escape rate k_e, which depends on the mass of the gas molecule

$$k_e = \frac{A_e}{V_c}\sqrt{\frac{k_B T}{2\pi m}} \tag{15}$$

In this study, the escape rate was measured for different pinhole sizes with inert gases of different masses. During the exposure of the substrate, the partial pressure in the Knudsen cell changes from p_0 (plunger closed) to p_r (plunger open) due to HCl uptake on the ice surface. Thus, the uptake onto the substrate is

$$R_S = \frac{k_e V_c}{k_B T}(p_0 - p_r) \tag{16}$$

Using the mean thermal velocity $\bar{v} = \sqrt{8k_B T/\pi m}$ and the gaskinetically maximal possible rate $R_{S,max} = A_S \bar{v} p_r / 4k_B T$ on the substrate during uptake, the uptake coefficient is

$$\gamma(t) = \frac{R_S}{R_{S,max}} = \frac{4k_e}{\bar{v}}\frac{V_c}{A_S}\frac{p_0 - p_r}{p_r} \tag{17}$$

From this equation, the temporal development of the partial pressure in the cell can be derived as

$$p_r(t) = \frac{p_0}{1 + \frac{\bar{v}A_S}{4k_e V_c}\gamma(t)} \tag{18}$$

Diffusive Uptake of a Nondissociating Species. For a gas with a bulk solubility H_d and a bulk phase diffusivity D, the diffusion equation can be solved in planar geometry assuming diffusion into an infinite reservoir and a constant partial pressure p_g in the gas phase.[81,112−115] Ignoring the initial time period of the uptake (i.e., for $t > (4H_d D^{1/2}/\alpha_c \bar{v})^2$, see ref 81), the flux density j through the interface is

$$j \simeq \frac{p_g}{k_B T}\frac{H_d\sqrt{D}}{\sqrt{\pi t}} \tag{19}$$

Using the flux density of an ideal gas (eq 6), the uptake coefficient for the diffusive process can be expressed as

$$\frac{1}{\gamma(t)} = \frac{\bar{v}}{4}\frac{\sqrt{\pi t}}{H_d\sqrt{D}} \tag{20}$$

This equation was used to determine $H_d D^{1/2}$ for HCl in sulfuric acid solutions under stratospheric conditions.[86] Using eq 18, the time dependence of the measured partial pressure in the cell is

$$p_r(t) = \frac{p_0}{1 + \frac{A_S}{V_c k_e}\frac{H_d\sqrt{D}}{\sqrt{\pi t}}} \tag{21}$$

Diffusive Uptake of a Dissociating Species. For a dissociating species, the solubility changes with the partial pressure p_r in the cell ($H_d^* = (k_B T_S K H_d / p_r)^{1/2}$). Using eqs 17 and 20, we find

$$\frac{1}{\gamma(t)}\sqrt{\frac{p_0}{p_r(t)}} = \frac{\bar{v}}{4}\sqrt{\frac{p_0}{k_B T_S K H_d}}\sqrt{\frac{\pi t}{D}} \tag{22}$$

The linear relation $1/\gamma(t) \times (p_0/p_r)^{1/2} \propto t^{1/2}$ can be used to determine $H_d^* D^{1/2} = (k_B T_S K H_d D/p_0)^{1/2}$ from the experimental data. The time dependence of the partial pressure p_r in the Knudsen cell is readily derived from eq 18

$$p_r(t) = p_0\left(1 + \frac{\zeta^2}{2t}\right) \pm \sqrt{p_0\left(1 + \frac{\zeta^2}{2t}\right) - {p_0}^2} \tag{23}$$

where

$$\zeta = \frac{A_S}{V_c k_e}\sqrt{\frac{k_B T_S K H_d}{p_0}}\sqrt{\frac{D}{\pi}} \tag{24}$$

The solutions for the diffusive uptake have a negative sign in eq 23. The positive branch would describe a source.

Note that the quantity $(k_B T_S K H_d D/p_0)^{1/2}$ corresponds to $H_d D^{1/2}$ in eq 20, which allows direct comparison. In this paper, $HD^{1/2}$ denotes the results calculated with eq 20, while results derived from eq 22 are denoted as $H_d^* D^{1/2}$ instead of using the full expression $(k_B T_S K H_d D/p_0)^{1/2}$.

Calculation of Total Uptake on the Substrate. The total uptake $n_{tot}(t)$ onto the substrate at time t is calculated by numerical integration of the rate of molecules taken up by the substrate (R_S in eq 16, using the experimentally measured p_0 and $p_r(t)$):

$$n_{tot}(t) = \int_{t'=0}^{t'=t} \frac{R_S(t')}{A_S} dt' \tag{25}$$

To estimate the diffusive contribution, $n_{diff}(t)$, to the overall uptake, we use the theoretical value for $p_r(t)$, as given in eq 21 or eq 23 in eq 25. The nondiffusive contribution $n_{resid}(t)$ to the overall uptake is given by the difference of total and diffusive uptake

$$n_{resid}(t) = n_{tot}(t) - n_{diff}(t) \tag{26}$$

Correction of Measured Partial Pressures Due to Temperature Differences in the Cell. The Hertz−Knudsen equation describes the net-flux through a surface with vapor pressure p_v in an ambient with partial pressure p_g. Under equilibrium conditions ($p_g = p_v$), the condensing flux $j_{cond} = \alpha_c p_g (2\pi m k_B T)^{-1/2}$ (cf. eq 6) must equal the evaporating flux. Thus, we have $j_{evap} = \alpha_c p_v (2\pi m k_B T)^{-1/2}$. Assuming that the evaporating and condensing fluxes are independent of each other, we can formulate the net flux, j_{net}, for nonequilibrium conditions (i.e., if $p_g \neq p_v$) and find the Hertz−Knudsen equation:

$$j_{net} = \alpha_c \frac{p_g}{\sqrt{2m k_B T_g}} - \alpha_c \frac{p_v}{\sqrt{2m k_B T_S}} \tag{27}$$

Note that we distinguish in eq 27 between the substrate and the gas temperatures T_S and T_g, respectively. This has a direct consequence for experiments performed on cold substrates in a reaction chamber with warm walls. Because the cell surface area is large compared to the cold substrate area, gas and cell temperatures T_S are equal. However, the evaporating molecules leave the ice at temperature T_S. Under equilibrium conditions (i.e., for $j_{net} = 0$, in eq 27), we find the relation between the pressure in the gas phase and the substrate vapor pressure[83]

$$p_g(T_c) = \sqrt{\frac{T_c}{T_S}}\, p_v(T_S) \tag{28}$$

Consequently, the measured partial pressure in the Knudsen cell (i.e., $j_{net} = 0$, i.e., $p_g = (T_c/T_S)^{1/2} p_v$), is higher than the ice vapor pressure. For a wall temperature of $T_c = 300$ K and $T_S = 200$ K, a 22% correction to the measured substrate vapor pressure must be applied. We have confirmed this simple correction by measuring the ice vapor pressures.

Appendix B: Numerical Model to Simulate Knudsen Cell Experiments

In this appendix, we describe the numerical model to simulate uptake experiments in the Knudsen cell. The model simulates the filling of the Knudsen cell, diffusion into the ice substrate, and the kinetics of surface adsorption. To formulate the model we use molecule densities and denote the density in the gas and ice phase as n_g and n_i, respectively (both in molecules m^{-3}), the concentration of adsorbed molecules as n_{surf} (in molec m^{-2}).

Surface Kinetics with Langmuir Adsorption. The HCl adsorbs on the surface and dissociates directly in a two stage process: HCl(g) $\rightleftharpoons$ HCl(ads) $\rightleftharpoons$ $Cl^- + H^+$. Assuming complete dissociation ($n_{surf,Cl^-} \cong n_{surf,H^+}$), the desorbing flux is $j_{des} = k_{surf,g} n_{surf,Cl^-} n_{surf,H^+} \approx k_{surf,g} n_{surf,Cl^2}$, and thus it is quadratic in the surface concentration. Here, $k_{surf,g}$ is the yet unknown desorption constant.

With eq 6 and the mean thermal velocity $\bar{v} = \sqrt{8k_B T/\pi m}$, we formulate the flux density $j_{g,surf} = \dot{n}_{surf}$ of the gas molecules entering the ice surface

$$j_{g,surf} = k_{g,surf}\, n_g \left(1 - \frac{n_{surf}}{n_{surf,max}}\right)^k \tag{29}$$

Here, $n_{surf,max}$ is the number of sites available for adsorption on the ice surface and we use the definition $k_{g,surf} = \alpha_c \bar{v}/4$. For a nondissociating species, we have $k = 1$, while for adsorption of a dissociating species one may chose $k = 2$.[91] However, given the low estimated surface coverage, the saturation term is mathematically unimportant. Even if we choose the maximum surface concentration $n_{surf,max}$ close to the maximum observed coverage, the influence of the term $(1 - n_{surf}/n_{surf,max})^k$ is negligible, compared to the overall accuracy of the experimental data. For practical matters, we have tested that the results presented in this study are independent from choosing $k = 1$ or $k = 2$. Thus, we have chosen $k = 1$ in all calculations and the reminder of this work.

The net flux, j_{net}, from the gas phase onto the surface is the difference between adsorbing and desorbing flux:

$$j_{net} = k_{g,surf}\, n_g \left(1 - \frac{n_{surf}}{n_{surf,max}}\right) - k_{surf,g}\, {n_{surf,Cl}}^j \tag{30}$$

Let $n_{surf,equi}$ be the total equilibrium concentration (i.e., adsorbed HCl and dissociated Cl^-) of HCl molecules taken up on the ice surface for the given gas-phase concentration $n_{g,0} = p_0/k_B/T$, with the plunger closed. In thermodynamic equilibrium, the adsorbing and desorbing fluxes must match, i.e., $j_{net} = 0$ in eq 30, and we express $k_{surf,g}$ as a function of the equilibrium surface coverage $n_{surf,equi}$ and the gas-phase concentration $n_{g,0}$ with closed plunger:

$$k_{surf,g} = k_{g,surf} \left(1 - \frac{n_{surf,equi}}{n_{surf,max}}\right) \frac{n_{g,0}}{{n_{surf,equi}}^j} \tag{31}$$

Thus, we can express the constant $k_{surf,g}$ as a function of the adsorption constant $k_{g,surf}$ and the equilibrium surface concentration $n_{surf,equi}$.

Mass Balance in the Gas Phase. To formulate the mass balance in the gas phase, we consider the loss rate from the gas phase onto the ice $-A_{ice}\alpha_c \bar{v}/4 \times (1 - n_{surf}/n_{surf,max})$, the desorption from the ice surface ($A_{ice}\, k_{surf,g}\, {n_{surf}}^j$), the gas flow into the Knudsen cell (R_{in}) and the loss into the mass spectrometer ($-k_e N_g$). We find the differential equation for the gas-phase concentration $n_g = N_g/V_c$

$$\frac{\partial n_g(t)}{\partial t} = -\frac{A_{ice}}{V_c} k_{g,surf}\, n_g \left(1 - \frac{n_{surf}}{n_{surf,max}}\right) + \frac{A_{ice}}{V_c} k_{surf,g}\, {n_s}^j - k_e n_g + \frac{R_{in}}{V_c} \tag{32}$$

Solution of the Diffusion Equation. For numerical solution of the diffusion equation, we convert this partial differential equation into a system of coupled ordinary differential equations by discretization of the spatial coordinates. The ice is modelled as a one-dimensional slab, which consists of equidistant boxes of length h. To formulate the mass balance in each box, we consider the continuity equation for the k^{th} cell at the coordinate x_k

$$\left.\frac{\partial n_i(x)}{\partial t}\right|_{x=x_k} = -\nabla \vec{j} = -\lim_{\Delta V \to 0} \frac{1}{\Delta V} \int_S \vec{j}\, d\vec{A}_S \tag{33}$$

Here, $\vec{j}$ is the flux density through the surface S of the volume $\Delta V = hA_S$. The diffusive flux from cell k at coordinate x_k into cell $k + 1$ (at $x_k + h$) is expressed by discretization of Fick's first law:

$$j = D \left.\frac{\partial n_i(x)}{\partial x}\right|_{x=x_k} \approx D \frac{n_i(x_k) - n_i(x_{k+1})}{h} \tag{34}$$

Using the analogous expression for the diffusion into cell $k - 1$ in the continuity eq 33 and the definition $k_D = Dh^{-2}$, we find

$$\frac{\partial n_i(x)}{\partial t} = k_D(n_i(x_{k+1}) - n_i(x_k)) + k_D(n_i(x_{k-1}) - n_i(x_k)) \tag{35}$$

for the discretization. By this procedure, the problem reduces to a system of coupled ordinary differential equations.

Two boundary conditions are needed for complete formulation of the problem. The first one is that the concentration gradient in the depth of the ice vanishes. The second boundary condition is based on the transport between the ice surface and the bulk. To describe the transport between the ice surface and the first box below the surface, we assume that the diffusive flux toward the surface is as fast as the diffusion between the

boxes in the bulk that is $j = k_D n_i(x = 0)$. Thus, the mass balance between ice surface and bulk reads

$$\frac{\partial n_i(x=0)}{\partial t} = k_D n_i(x=0) - k_{surf,i}\, n_{surf} \qquad (36)$$

where the unknown $k_{surf,i}$ is determined by considering the thermodynamic equilibrium, that is $\partial n_i(x = 0)/\partial t = 0$ or $k_{surf,i} = k_D n_{i,equi}/n_{surf,equi}$. Using Henry's law, $H_d n_{g,0} = n_{i,equi}$, we can express $k_{surf,i}$ as a function of the Henry's law constant H_d, the equilibrium surface coverage $n_{surf,equi}$ and the gas-phase concentration with closed plunger $n_{g,0}$:

$$k_{surf,i} = k_D \frac{H_d n_{g,0}}{n_{surf,equi}} \qquad (37)$$

Differential Equation for the Ice Surface. Analogously, we formulate the differential equation for the ice surface:

$$\frac{\partial n_{surf}}{\partial t} = k_{g,surf}\, n_g \left(1 - \frac{n_{surf}}{n_{surf,max}}\right) + k_{surf,g}\, n_{surf}^{\ j} + \frac{V_c}{A_{ice}}(k_D n_i(x=0) - k_{surf,i}\, n_s) \qquad (38)$$

In summary, eqs 32, 35, and 38 with $k_D = Dh^{-2}$, $k_{g,surf} \equiv \alpha_c \bar{v}/4$, and the expressions for $k_{surf,g}$ and $k_{surf,i}$ (eqs 31 and 37) are a system of coupled first-order differential equations. The system describes the kinetics in the Knudsen cell as a function of the equilibrium surface concentration $n_{surf,equi}$ (or the equilibrium coverage $\theta_{equi} = n_{surf,equi}/n_{surf,max}$), the saturation concentration on the surface is $n_{surf,max}$, the Henry's law constant H_d, and the diffusion constant D. Diffusive processes are governed by the product $H_d D^{1/2}$.[81,115] Variation of H_d did not affect the result for $H_d D^{1/2}$ or θ_{equi}. Furthermore, the choice of $n_{surf,max}$ has negligible influence on the overall results, thus the two parameters $H_d D^{1/2}$ and the equilibrium coverage $\theta_{equi} = n_{surf,equi}/n_{surf,max}$ effectively govern the overall kinetics.

The system of coupled differential equations is numerically stiff. Therefore, for numerical solution, we use a code based on backward differencing formulas, originally developed by Gear[116,117] in an implementation in the PV-Wave software package.[118]

Acknowledgment. We would like to thank Drs. T. Hickmott and J. N. Crowley for valuable comments on the manuscript, Drs. J. Kimball, K. J. Lee, and W. A. Lanford for discussion of the surface kinetics on the ice surface. We would like to thank Prof. K. Heinloth for helpful discussions during the course of this project, and we appreciate the valuable comments of the anonymous reviewers. We are deeply indebted to Gerhard Schuster for his exceptional technical and practical support to this work. Parts of this work have been funded from Project 01L09526 of the German BMBF.

References and Notes

(1) Solomon, S. *Nature (London)* **1990**, *347*, 347−353.
(2) Legrand, M. R.; Delmas, R. L.; Charlson, R. J. *Nature (London)* **1988**, *334*, 418−420.
(3) Barnola, J. M.; Raynaud, D.; Korotkevich, Y. S.; Lorius, C. *Nature (London)* **1987**, *329*, 408−414.
(4) Wolff, E. W. Location, movement and reaction of impurities in solid ice. In *Chemical Exchange between the atmosphere and polar snow*; NATO ASI Series. Series I: Global environmental change; Wolff, E. W., Bales, R. C., Eds.; Springer: Berlin, 1995; Vol. 43.
(5) Schwartz, S. E.; Freiberg, J. E. *Atmos. Environ.* **1981**, *15*, 1129−1144.
(6) Schwartz, S. E. *Mass-transport considerations pertinent to aqueous phase reactions of gases in liquid-water clouds*; NATO ASI Series G6, Chemistry of Multiphase Atmospheric Systems; Springer-Verlag: Berlin, and Heidelberg, Germany, 1986.
(7) Hanson, D. R.; Ravishankara, A. R.; Solomon, S. *J. Geophys. Res.* **1994**, *99, D2*, 3615−3629.
(8) Hanson, D. R. *J. Phys. Chem. B* **1997**, *101*, 4998−5001.
(9) Elliot, S. E.; Turco, R. P.; Toon, O. B.; Hamill, P. *J. Atmos. Chem.* **1991**, *13*, 211−224.
(10) Tabazadeh, A.; Turco, R. P. *J. Geophys. Res.* **1993**, *98D7*, 12727−12740.
(11) Ravishankara, A. R. *Science* **1997**, *276*, 1058−1065.
(12) Carslaw, K. S.; Peter, Th. *Geophys. Res. Lett.* **1997**, *24* (14), 1743−1746.
(13) Abbatt, J. P. D. *Chem. Rev.* **2003**, *103*, 4783−4800.
(14) Krishnan, P. N.; Salomon, R. E. *J. Phys. Chem.* **1969**, *73*, 2680−2683.
(15) Seidensticker, R. G. *J. Chem. Phys.* **1972**, *56*, 2853−2857.
(16) Gross, G. W.; Wu., C.; Bryant, L.; McKee, C. *J. Chem. Phys.* **1975**, *8*, 3085−3092.
(17) Elliot, S. E.; Turco, R. P.; Toon, O. B.; Hamill, P. *Geophys. Res. Lett.* **1990**, *17*, 425−428.
(18) Dominé, F.; Thibert, E. *Geophys. Res. Lett.* **1996**, *24*, 3627−3630.
(19) Thibert, E.; Dominé, F. *J. Phys. Chem. B* **1997**, *101*, 3554−3565.
(20) Thibert, E.; Dominé, F. *J. Phys. Chem.* **1998**, *102*, 4432−4439.
(21) Caloz, F.; Fenter, F. F.; Tabor, K. D.; Rossi, M. J. *Rev. Sci. Instrum.* **1997**, *68*, 3172−3179.
(22) Flückiger, B.; Chaix, L.; Rossi, M. *J. Phys. Chem. A* **2000**, *104*, 4432−4439.
(23) Barone, S.; Zondlo, M. A.; Tolbert, M. *J. Phys. Chem.* **1999**, *103*, 9717−9730.
(24) Flückiger, B.; Rossi, M. *J. Phys. Chem. A* **2003**, *107*, 4103−4115.
(25) Abbatt, J. P. D.; Beyer, K. D.; Fucaloro, A. F.; McMahon, J. R.; Wooldridge, P. J.; Zhang, R.; Molina, M. J. *J. Geophys. Res.* **1992**, *97D14*, 15918−15826.
(26) Hanson, D. R.; Ravishankara, A. R. *J. Phys. Chem.* **1992**, *96*, 2682−2691.
(27) Chu, L. T.; Leu, M. T.; Keyser, L. F. *J. Phys. Chem.* **1993**, *97*, 7779−7785.
(28) Leu, M. T.; Keyser, L. F.; Timonen, R. S. *J. Phys. Chem. B* **1997**, *101*, 6259−6262.
(29) Foster, K. L.; Tolbert, M. A.; George, S. M. *J. Phys. Chem.* **1997**, *101*, 4979−4986.
(30) Hynes, R. G.; Mössinger, J. C.; Cox, R. A. *Geophys. Res. Lett.* **2001**, *28*, 2827−2830.
(31) Hanson, D.; Mauersberger, K. *Geophys. Res. Lett.* **1988**, *15, No 13*, 1507−1510.
(32) Keyser, L. F.; Leu, M. T. *Microsc. Res. Technol.* **1993**, *25*, 434−438.
(33) Keyser, L. F.; Leu, M. T. *J. Colloid Interface Sci.* **1993**, *155*, 137−145.
(34) Keyser, L. K.; Leu, M. T.; Moore, S. B. *J. Phys. Chem.* **1993**, *97*, 2800−2801.
(35) Hanson, D. R.; Ravishankara, A. R. *J. Phys. Chem.* **1993**, *97*, 2802−2803.
(36) Sadtchenko, V.; Giese, C. F.; Gentry, W. *J. Phys. Chem. B* **2000**, *104*, 9421−9429.
(37) Abbatt, J. P. D.; Molina, M. J. *J. Phys. Chem.* **1992**, *96*, 7674−7679.
(38) Abbatt, J. P. D. *Geophys. Res. Lett.* **1997**, *24*, 1479−1482.
(39) Clapsaddle, C.; Lamb, D. *Geophys. Res. Lett.* **1989**, *16*, 1173−1176.
(40) Conklin, M. H.; Sommerfeld, R. A.; Laird, S. K.; Villinski, J. E. *Atmos. Environ.* **1993**, *27A*, 159−166.
(41) Clegg, S. M.; Abbatt, J. P. D. *J. Phys. Chem. A* **2000**, *105*, 6630−6636.
(42) Chu, L.; Diao, G. W.; Chu, L. T. *J. Phys. Chem. A* **2000**, *104*, 7565−7573.
(43) Conklin, M. H.; Sigg, A.; Neftel, A. *J. Geophys. Res.* **1993**, *98*, 18367−18376.
(44) Huthwelker, T.; Lamb, D.; Baker, M.; Swanson, B.; Peter, Th. *J. Colloid Interface Sci.* **2001**, *238*, 147−159.
(45) Dosch, H. *Critical phenomena at surfaces and interfaces*; Springer Tracts in modern Physics 126; Springer: Berlin, Heidelberg, Germany, and New York, 1992.
(46) Golecki, I.; Jaccard, C. *Phys. Lett. A* **1977**, *63*, 374−376.
(47) Kouchi, A.; Furukawa, Y.; Kuroda, T. *J. Phys. (Paris) C1* **1987**, *48*, C1−676.
(48) Beaglehole, D. *J. Cryst. Growth* **1991**, *112*, 663−669.
(49) Elbaum, M.; Schick, M. *Phys. Rev. Lett.* **1991**, *66*, 1713−1716.
(50) Lied, A.; Dosch, H.; Bilgram, J. H. *Physica* **1994**, *B 198*, 92−96.
(51) Lied, A.; Dosch, H.; Bilgram, J. H. *Phys. Rev. Lett.* **1994**, *72*, 3554−3557.

(52) Dosch, H.; Lied, A.; Bilgram, J. H. *Surf. Sci.* **1995**, *327*, 145−164.
(53) Dash, J. G.; Fu, H.; Wettlaufer, J. S. *Rep. Prog. Phys.* **1995**, *58*, 115−167.
(54) Wei, X.; Miranda, P.; Shen, Y. *Phys. Rev. B* **2002**, *66*, art. no. 085401.
(55) Diehl, K.; Mitra, S. K.; Pruppacher, H. R. *Atmos. Env.* **1995**, *29*, 975−981.
(56) Conklin, M. H.; Bales, R. C. *J. Geophys. Res.* **1993**, *98*, 16851−16855.
(57) Molina, M. J. In *Chemistry of the atmosphere: Its impact on global change*; Calvert, J. G., Ed.; Blackwell Sci.: Oxford, U.K., 1994.
(58) Chen, J. P.; Crutzen, P. J. *J. Geophys. Res.* **1994**, *99D9*, 18847−18859.
(59) Diehl, K.; Mitra, S. K.; Pruppacher, H. R. *Atmos. Res.* **1998**, *47*−*48*, 235−244.
(60) Knight, C. A. *J. Geophys. Res.* **1996**, *101*, *D8*, 12933−12936.
(61) Baker, M. B.; Dash, J. G. *J. Geophys. Res.* **1996**, *101 D8*, 12929−12931.
(62) Knight, C. A. *J. Geophys. Res.* **1996**, *101*, 12921−12928.
(63) Baker, M.; Nelson, J. *J. Geophys. Res.* **1996**, *102 D17*, 23035−23038.
(64) Paren, J. G.; Walker, J. C. F. *Nature: Phys. Sci.* **1971**, *230*, 77−79.
(65) Mader, H. *J. Glaciology* **1992**, *38*, 359−374.
(66) Mader, H. *J. Glaciology* **1992**, *38*, 333−347.
(67) Colbeck, S. C. *J. Colloid Interface Sci.* **1979**, ***72***, *3*, 371−384.
(68) Mulvany, R.; Wolff, E. W.; Oates, K. *Nature (London)* **1988**, *331*, 247−249.
(69) Wolff, E. W.; Mulvaney, R.; Oates, K. *Geophys. Res. Lett.* **1989**, *16*, 487−490.
(70) Banham, S. F.; Horn, A. B.; Koch, T. G.; Sodeau, J. R. *Faraday Discuss.* **1995**, *100*, 123−128.
(71) Horn, A. B.; Sodeau, J. R.; Roddis, T. B.; Williams, N. A. *J. Phys. Chem. A* **1998**, *102*, 6107−6120.
(72) Bianco, R.; Thompson, W. H.; Morita, A.; Hynes, J. T. *J. Phys. Chem. A* **2001**, *105*, 3132−3139.
(73) Hudson, P. K.; Shilling, J. E.; Tolbert, M. A.; Toon, O. B. *J. Phys. Chem. A* **2002**, *106*, 9874−9882.
(74) Devlin, J. P.; Uras, N.; Sadlej, J.; Buch, V. *Nature (London)* **2002**, *417*, 269−271.
(75) Bolton, K.; J. B. C. Pettersson, J. *J. Am. Chem. Soc.* **2001**, *123*, 7360−7363.
(76) Gertner, B. J.; Hynes, J. T. *Science* **1996**, *271*, 1563−1566.
(77) Adamson, A. W. *Physical chemistry of surfaces*; John Wiley and Sons: New York, 1990.
(78) Adamson, A. W.; Dormant, L. M.; Orem, M. *J. Colloid Interface Sci.* **1967**, *25*, 206−217.
(79) Orem, M. W.; Adamson, A. W. *J. Colloid Sci.* **1969**, *31*, No. 2, 278−286.
(80) Mozurkewich, M. *Geophys. Res. Lett.* **1993**, *20*, 355−358.
(81) Huthwelker, T.; Peter, Th. *J. Chem. Phys.* **1996**, *105*, 1661−1667.
(82) Helleis, F. *F−Surf: Software and electronics for real-time measurements of mass spectrometer signals*; Max-Planck-Institute for Chemistry: Mainz, Germany, 1997.
(83) Huthwelker, T. *Experimente und Modellierung der Spurengasaufnahme*; Eis. Dissertation, Universität Bonn; Cuvillier Verlag: Göttingen, Germany, 1999; ISBN 3-89712-675-3.
(84) McDonald, J. E. *J. Geophys. Res.* **1965**, *70*, 1553−1554.
(85) Because this systematic error affects all pressure measurements equally, it will not affect the observed pressure dependence of the uptake, thus it is not added to the errorbars in Figure 6a,b. However, the systematic error affects the position of our data relative to the ice phase boundary (at 1.3×10^{-5} Torr HCl for 203 K, after Carslaw et al.[90]). This error is marked as a dotted line in Figures 6 and 7.
(86) Williams, L. R.; Golden, D. M. *Geophys. Res. Lett.* **1993**, *20*, 2227−2230.
(87) We note that Hanson and Mauersberger[94] observed increasing HCl uptake on cold glass with rising humidity. They determined an HCl uptake of 6×10^{13} cm^{-2} on **cold** glass surfaces at water partial pressures of 1.2 mTorr. This would lead to a higher value of 2×10^{14} cm^{-2} for the detection limit in our system. However, the additionally exposed glass surface in our system is mostly at room temperature or has a temperature gradient from room temperature to the substrate temperature. Thus, the Hanson and Mauersberger data are not applicable to our system. The comparison with the sulfuric acid data and the vanishing surface contribution at very high HCl vapor pressures is a more appropriate measurement of the additional wall-induced HCl uptake in our setup.
(88) Tabazadeh, A.; Toon, O. B.; Jensen, E. J. *Geophys. Res. Lett.* **1999**, *2614*, 2211−2214.
(89) In this calculation we have set θ_{equi} to a very low value, because the choice $\theta_{equi} = 0$ would prevent any transport from the gas phase into the bulk ice.
(90) Carslaw, K. S.; Clegg, S. L.; Brimblecombe, P. *J. Phys. Chem.* **1995**, *99*, 11557−11574.
(91) Trapnell, B. M. W. *Chemisorption;* Butterworth Scientific Publications: London, 1955.
(92) Lee, S.-H.; Leard, D. C.; Zhang, R. Z.; Molina, L. T.; Molina, M. J. *Chem. Phys. Lett.* **1999**, *315*, 7−11.
(93) This interpretation is in opposition to the interpretation of Hanson and Ravishankara,[26] who observed a reversible and an irreversible channel for the uptake. In their study, the surface uptake was considered reversible, while the dissolution into the bulk was not. This was concluded from a cycle of subsequent absorption and desorption in a flow tube experiment. We note, that absorption−desorption cycle are symmetric for merely diffusive processes, as has been demonstrated for the diffusion of HCl into sulfuric acid.[123] Thus, we suggest that the irreversible part must be caused by surface processes.
(94) Hanson, D. R.; Mauersberger, K. *J. Phys. Chem.* **1990**, *94*, 4700−4705.
(95) Clegg, S. M.; Abbatt, J. P. D. *Atmos. Chem. Phys.* **2001**, *1*, 73−78.
(96) Keyser, L. F.; Moore, S. B.; Leu, M. T. *J. Phys. Chem.* **1991**, *95*, 5496−5502.
(97) Luo, B. P.; Clegg, S. L.; Peter, Th.; Müller, R.; Crutzen, P. J. *Geophys. Res. Lett.* **1994**, *21*, 49−52.
(98) The high diffusion constant $D = 10^{-13}$ m^2 s^{-1} at 185 K may be excluded, as these data were taken at HCl partial pressures high enough to melt the ice.[25,122] Also, the higher values from Krieger et al.[110] do not reflect the diffusivity in the ice matrix, as these data were taken from a frozen doped solution with HCl mixing ratio was clearly above the solubility limit in ice. The upper limit of 10^{-14} m^2 s^{-1} as given by Wolff[69] might also be too high as it was measured in the ice surrounding a triple junction, which was filled with a liquid HCl solution. As such a system is thermodynamically exactly at the triple point, i.e., very close to melting conditions, the speed of diffusion might have been overestimated. Similar arguments might apply to the data of Krishanan and Salomon.[14] All other diffusion constant with values $D > 10^{-16}$ m^2 s^{-1} have been measured at higher temperatures.
(99) As the mean free path is larger than the pore size, as phase molecules enter pores by adsorbing on and desorbing from the pore walls. This process is called Knudsen diffusion.
(100) Van Genuchten, M. T.; Wirenga, P. J. *J. Soil. Sci. Soc. Am.* **1976**, *40*, 473−480.
(101) Nye, J. F. *J. Glaciol* **1991**, *37* (127), 401−413.
(102) Fukazawa, H.; Sugiyama, K.; Mae, S. *J. Phys. Chem.* **1998**, *102*, 4794−4807.
(103) Wettlaufer, J. S. *Phys. Rev. Lett.* **1999**, *83*, 2516−2519.
(104) Buch, V.; Delzeit, L.; Blackledge, C.; Devlin, J. P. *J. Phys. Chem.* **1996**, *100*, 3732−3744.
(105) Delzeit, L.; Rowland, B.; Devlin, J. P.; Buch, V. *J. Phys. Chem.* **1996**, *100*, 10076−10082.
(106) Devlin, J. P.; Buch, V. *J. Phys. Chem. B* **1997**, *101*, 6095−6098.
(107) Devlin, J. P.; Uras, N.; Rahman, M.; Buch, V. *Isr. J. Chem.* **1999**, *39*, 261−272.
(108) Delzeit, L.; Devlin, J. P.; Buch, V. *J. Chem. Phys.* **1997**, *107*, 3726−3729.
(109) Livingston, F. E.; George, S. M. *J. Phys. Chem. A* **2001**, *105*, 5155−5165.
(110) Krieger, U. K.; Huthwelker, T.; Daniel, C.; Weers, U.; Peter, Th.; Lanford, W. *Science* **2002**, *295*, 1048−1050.
(111) Huthwelker, T.; Krieger, U.; Weers, U.; Peter, Th.; Lanford, W. *Nucl. Instrum. Methods Phys. Res. B* **2002**, *B 190*, 47−53.
(112) Danckwerts, P. V. *Trans. Faraday Soc.* **1951**, *47*, 1014−1023.
(113) Crank, J. *Mathematics of diffusion;* Oxford University Press: London, 1956.
(114) Carslaw, H. S.; Jaeger, J. C. *Conduction of heat in solids;* Clarendon Press: Oxford, U.K., 1959.
(115) Danckwerts, P. V. *Gas−liquid reactions*; McGraw-Hill Chemical Engineering Series; McGraw-Hill: New York, 1970.
(116) Gear, C. *Numerical initial value problems in ordinary differential equations*; Prentice-Hall: London, 1971.
(117) Gear, C. W. *Commun. ACM* **1971**, *14*, 176−179.
(118) PV−Wave. *PV−WAVE command language with IMSL-Library extension;* Visual Numerics, Inc.: San Ramon, CA, 1994.
(119) Barnaal, D.; Slotfeldt-Ellingsen, D. *J. Phys. Chem.* **1983**, *87*, 4321−4325.
(120) Dominé, F.; Thibert, E.; Landeghem, F. V.; Silvente, E.; Wagnon, P. *Geophys. Res. Lett.* **1994**, *21*, 601−604.
(121) Huthwelker, T.; Krieger, U. K.; Peter, Th.; Lanford, W. In *Proccedings of the 17th International Conference on the Application of Accelerator in Research and Industry*; Duggan, J. L., Morgan, I. L., Eds.; American Institute of Physics: Denton, TX, 2002; pp 400−403.
(122) Molina, M. J.; Tso, T. L.; Molina, L. T.; Wang, F. C. Y. *Science* **1987**, *238*, 1253−1257.
(123) Hanson, D. R.; Ravishankara, A. R. *J. Phys. Chem.* **1993**, *97*, 12309−12319.